3. Indirect methods

- **Micro/nano-diffraction**
  - **Monochromatic beam (Bragg)**
  - **Polychromatic (Laue, differential-aperture)**
- **Coherent diffractive imaging**
  - **Isolated sample**
  - **Extended sample**
- **Holography**
- **Ultrafast imaging**

References:

1. J. Als-Nielsen and D. McMorrow, *Elements of Modern X-ray Physics* (Wiley, New York, 2000).
2. F. van der Veen and F. Pfeiffer, "Coherent x-ray scattering," J. Phys. Condens. Mat. 16, 5003 (2004).
3. J.R. Fienup, "Phase retrieval algorithms: a comparison," Appl. Opt. 21, 2758 (1982)
4. I. Robinson and R. Harder, "Coherent X-ray diffraction imaging of strain at the nanoscale," Nature Mater. 8, 291 (2009)
5. J. Stöhr and H.C. Siegmann, *Magnetism* (Springer, Berlin, 2006).

A change in the lattice constant introduces a shift in the Bragg spot

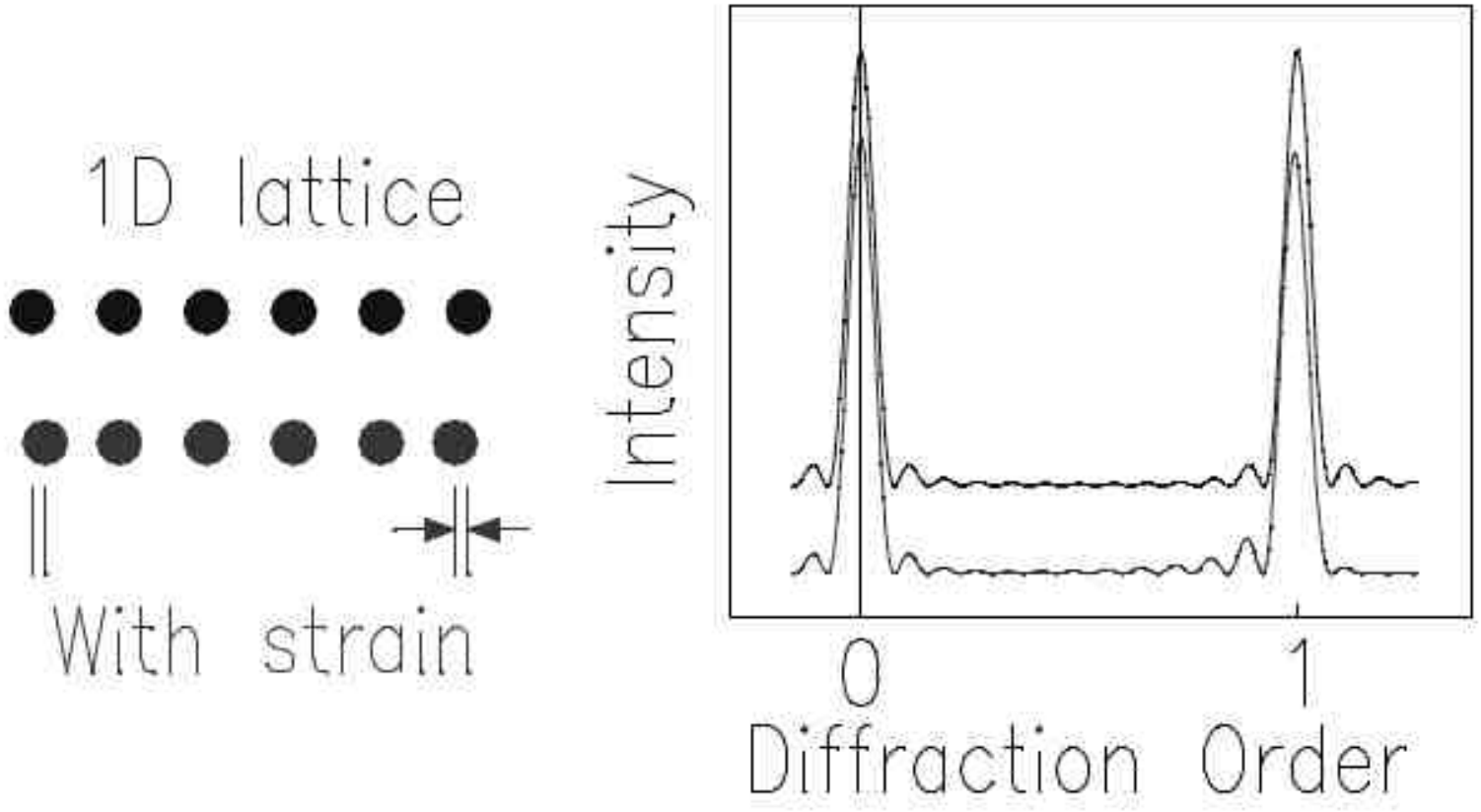

X-ray nano-diffraction

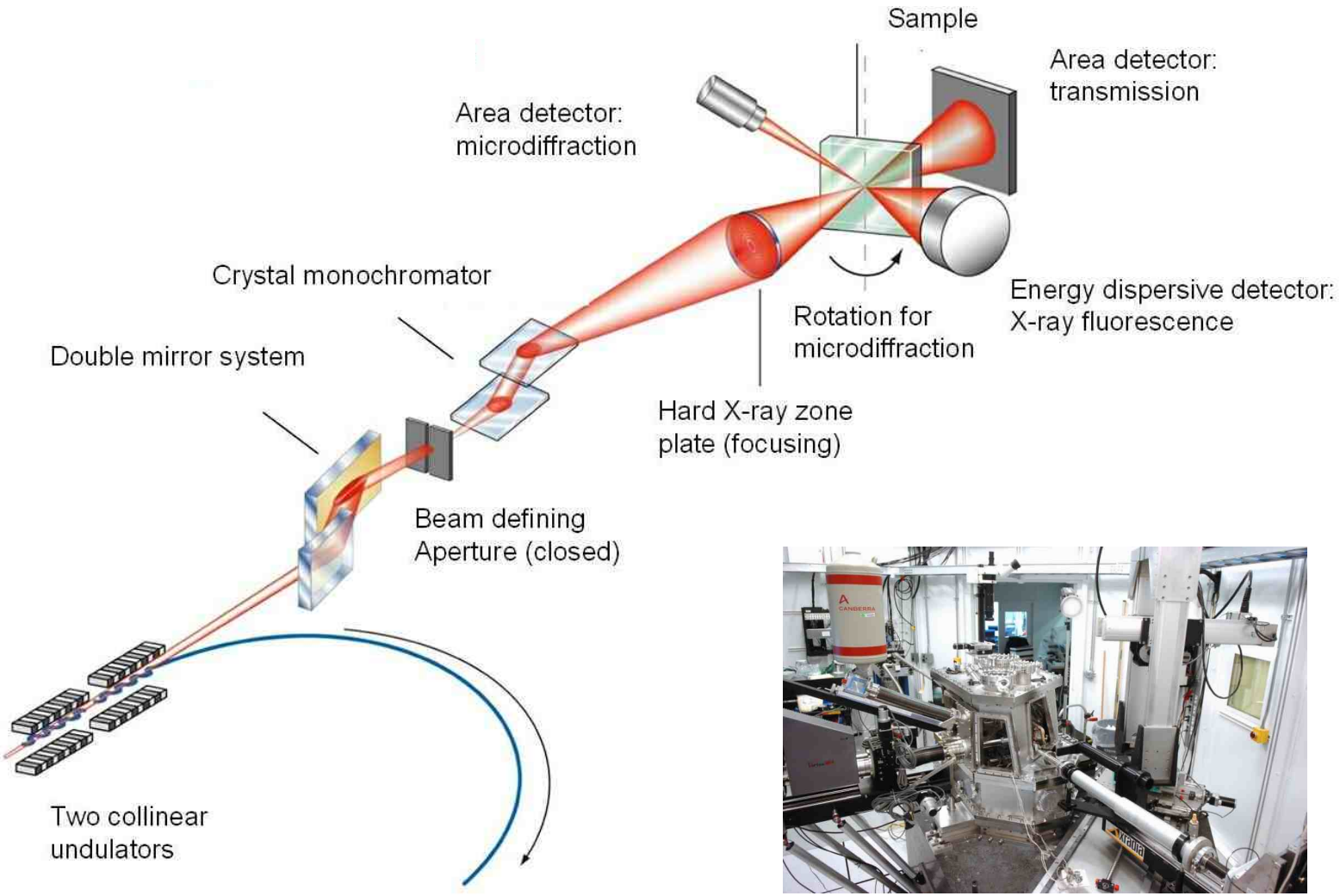

Hard X-ray Nanoprobe at APS 26-ID beamline

Microdiffraction reveals lattice strain in SOI structures

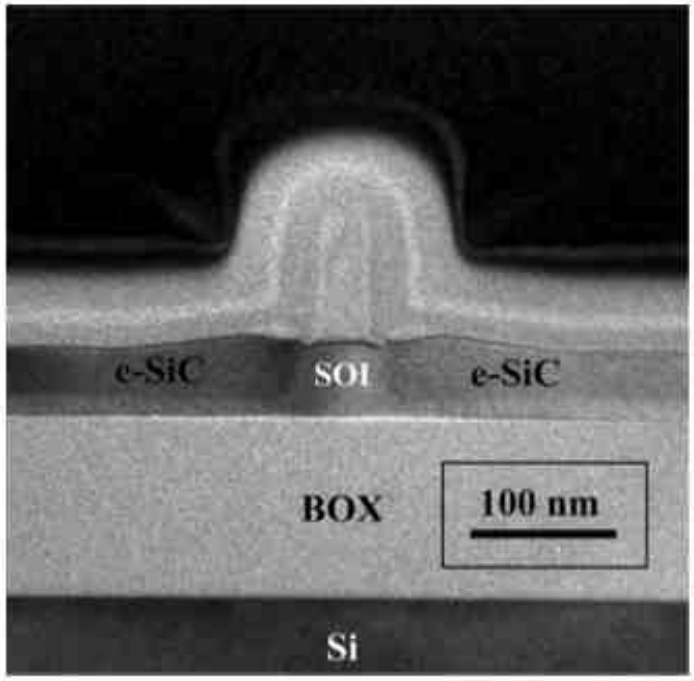

FIG. 2. Cross-sectional TEM image of e-SiC/SOI channel device.

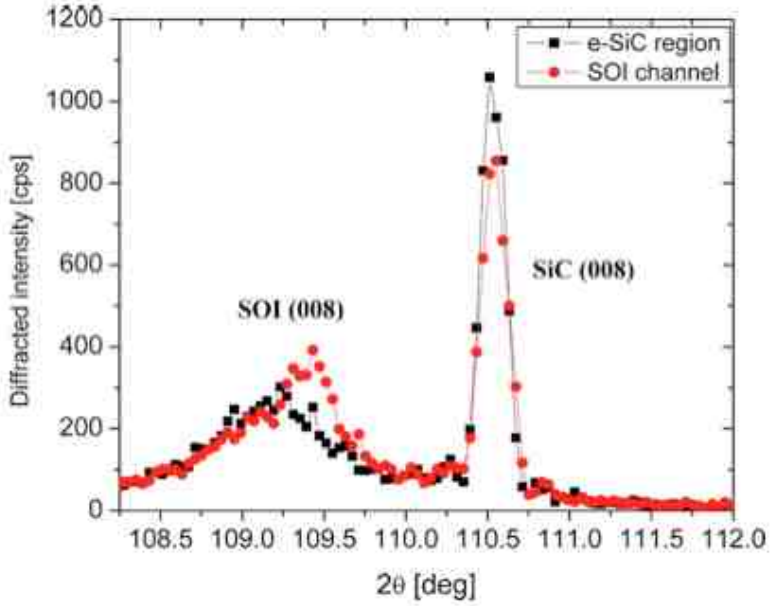

FIG. 3. (Color online) Comparison of the (008) diffraction measurements conducted at the SOI channel (red curve) and 0.8 μm away from channel (black curve).

C. Murray, APL 94, 063502 (2009)

… and the metal-insulator transition in VO_2

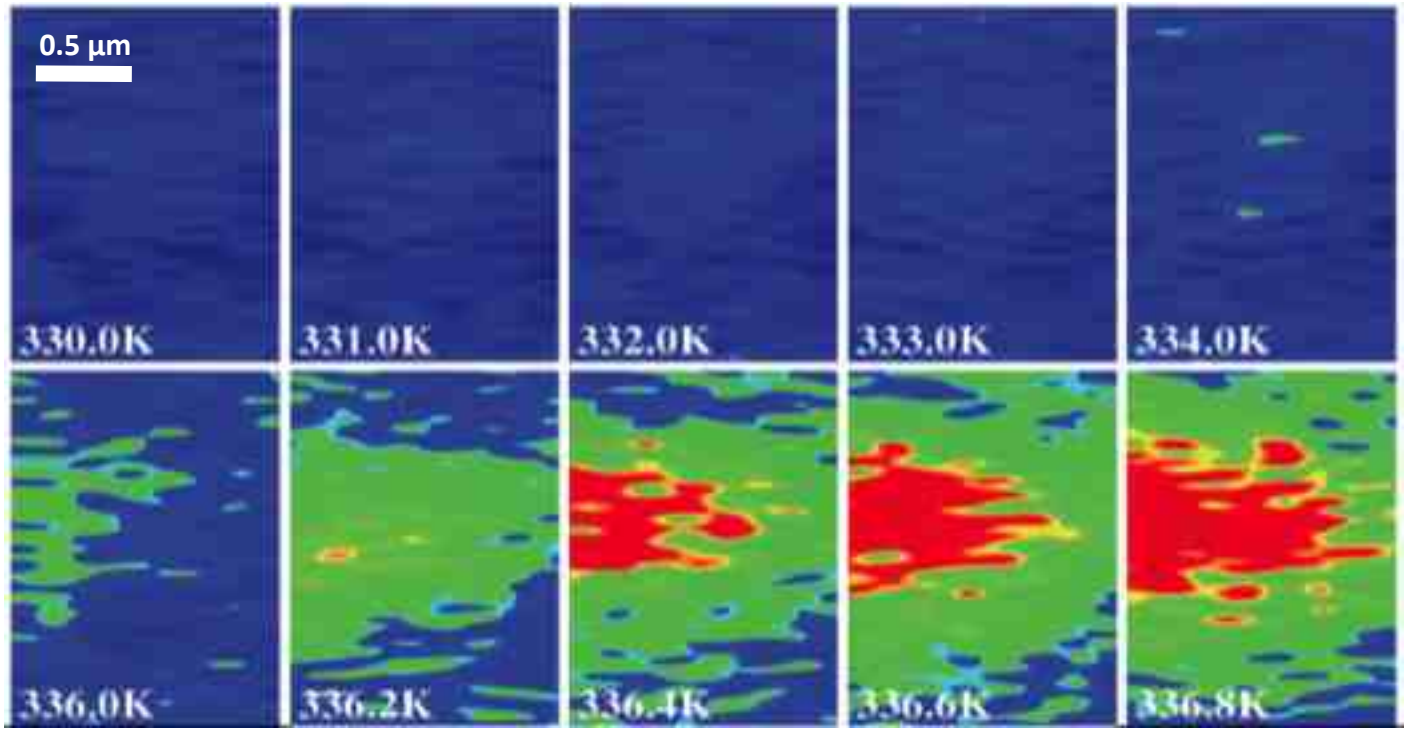

Spatial maps of the same 1.2 µm × 1.7 µm area, showing variation in the Bragg peak intensity from the M1 (monoclinic) phase of VO_2 during heating. Higher intensities (dark blue) indicate presence of the M1 phase, lower intensities (red) represent the rutile phase.

Both electronic and structural transitions evolve in a percolative manner, but the lattice switches *abruptly and non-monotonically* (not seen by near-field IR).

M. Qazilbash, PRB 83, 165108 (2011)

Electric field stabilization of domain walls is important for development of ultralow power electronic devices

- Predicting the properties of domain walls in multiferroic $BiFeO_3$ thin films requires detailed understanding of local and long-range lattice strain
- Linear domain response to interdigitated electrodes induces nanoscale lattice tilts (~100 nm domains)
- This can be measured within the electrode region with hard x-ray nano-diffraction

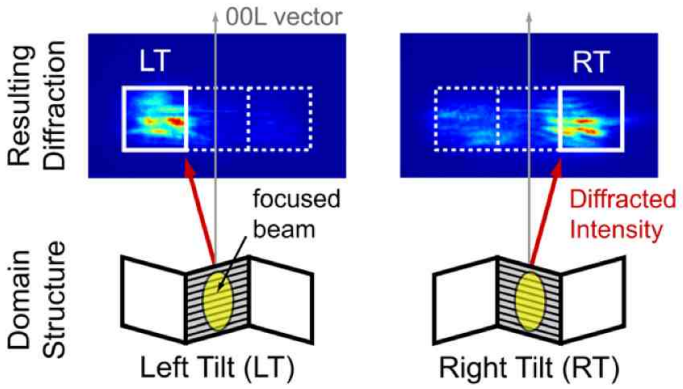

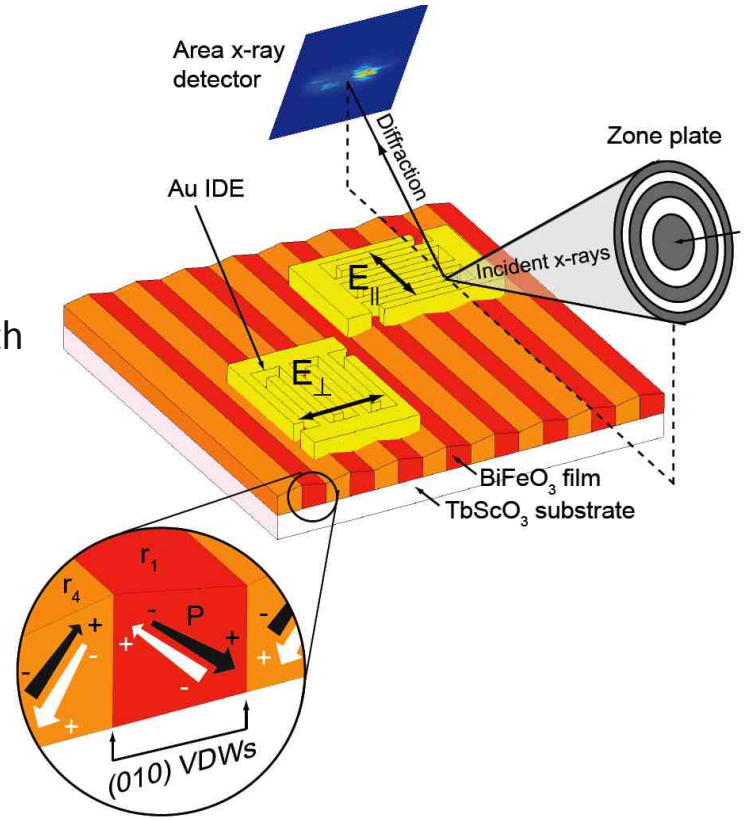

Lattice tilt domains in $BiFeO_3$ occur on the nanometer scale

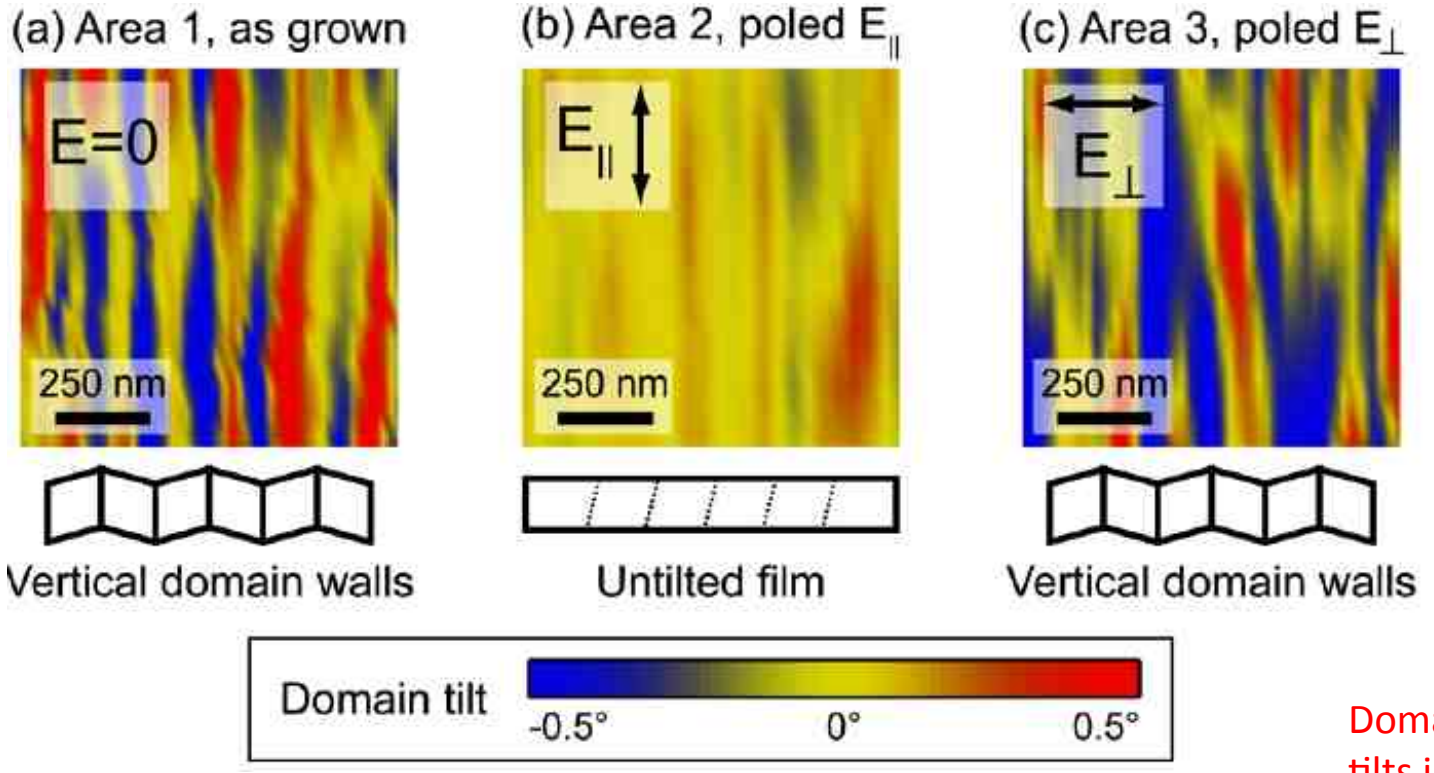

Domains switch tilts in < 20 nm !

Response of ferroelastic domains to E-field, poling parallel and perpendicular to as-grown state

S. Hruszkewycz, APL 99, 232903 (2011)

Differential-aperture x-ray microscopy

3D depth-resolved, white-beam Laue diffraction technique

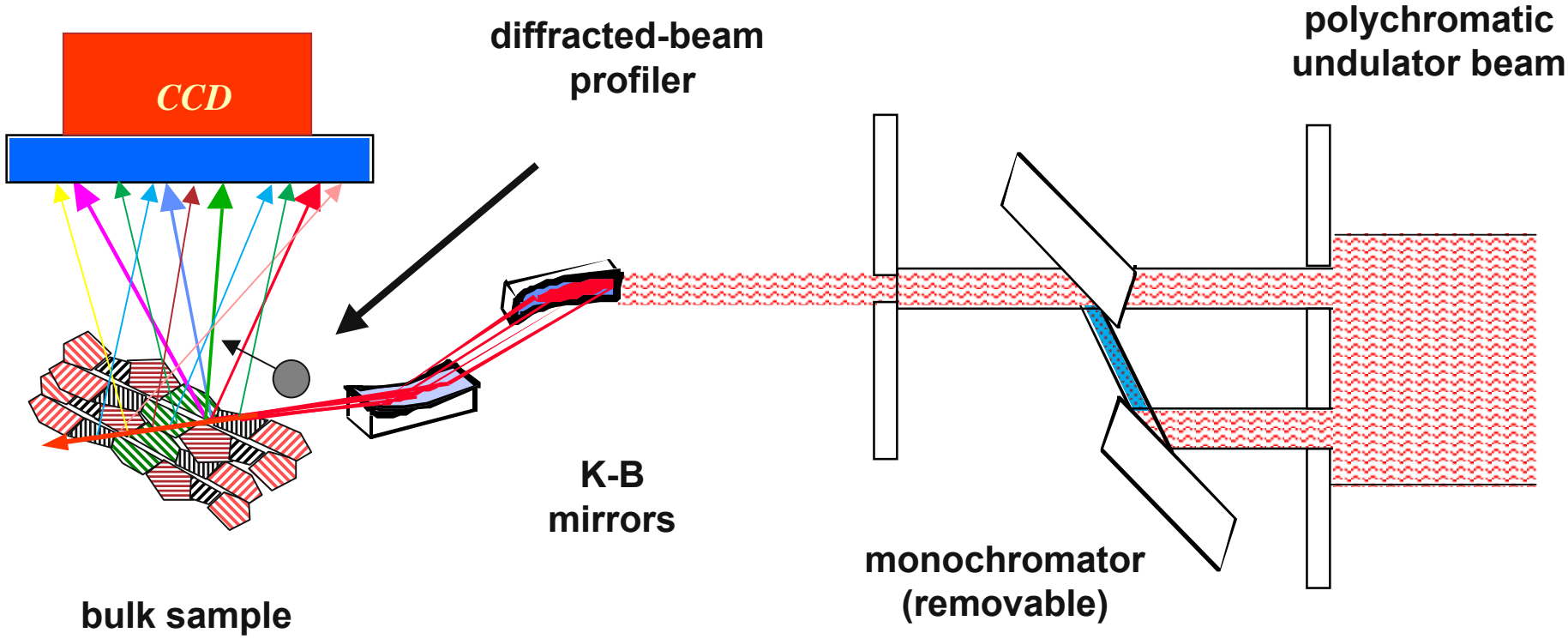

B. Larson, *Nature* 415, 887 (2002)

3D diffraction microscopy: how does it work?

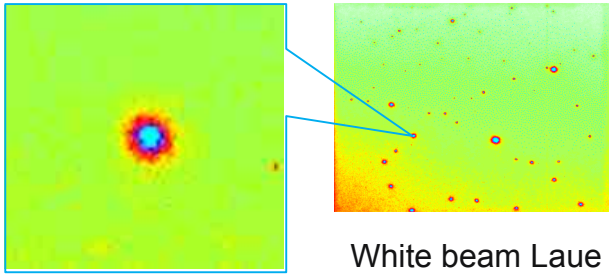

White beam Laue

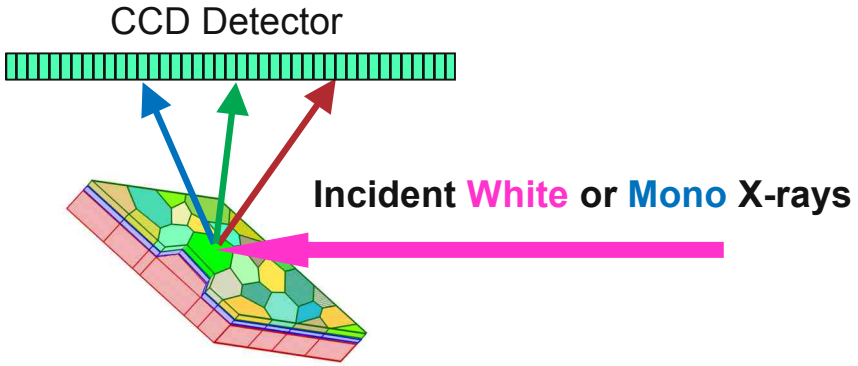

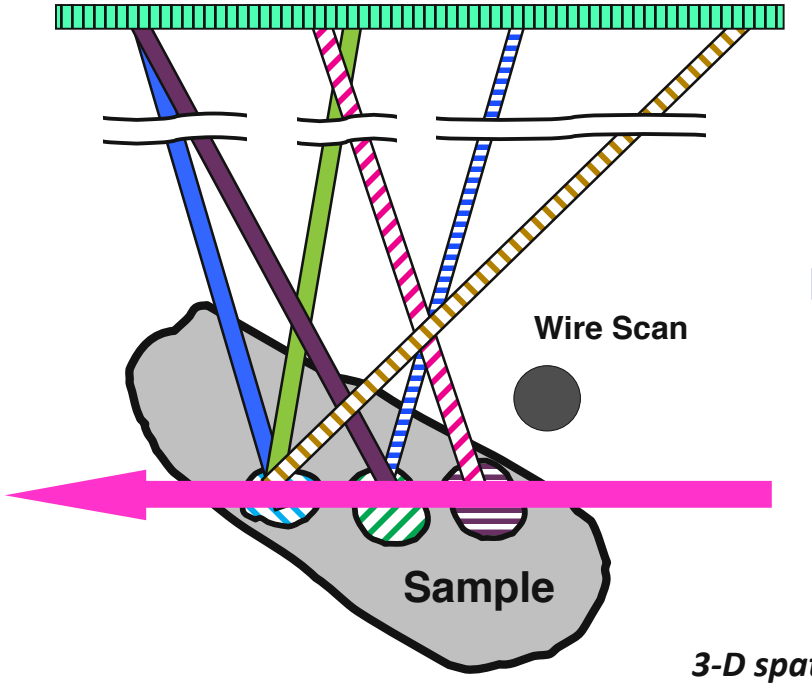

Depth profiling

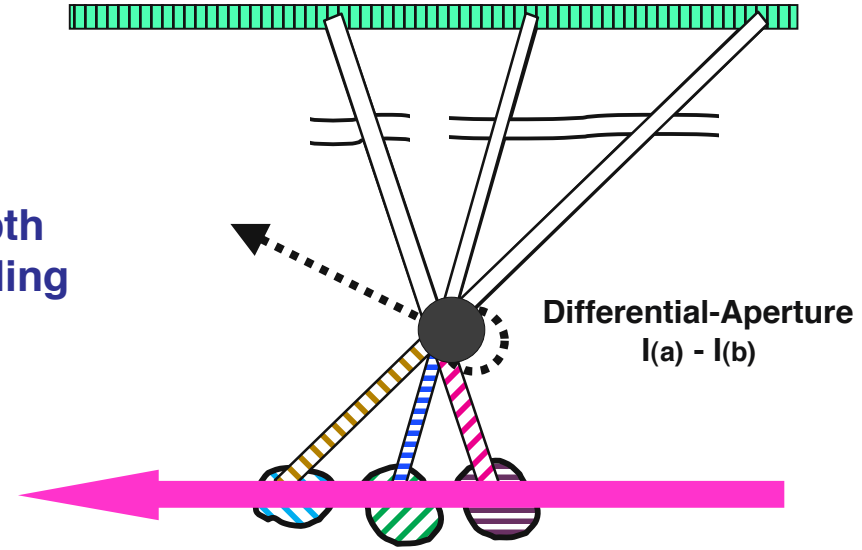

3-D spatial resolution: ~ 0.5 × 0.5 × 0.7 μm³

Angular resolution: Δϑ ~ 0.01° (orientation); Δd/d ~ 10⁻⁴ (strain)

3D diffraction microscope at APS beamline 34-ID-E

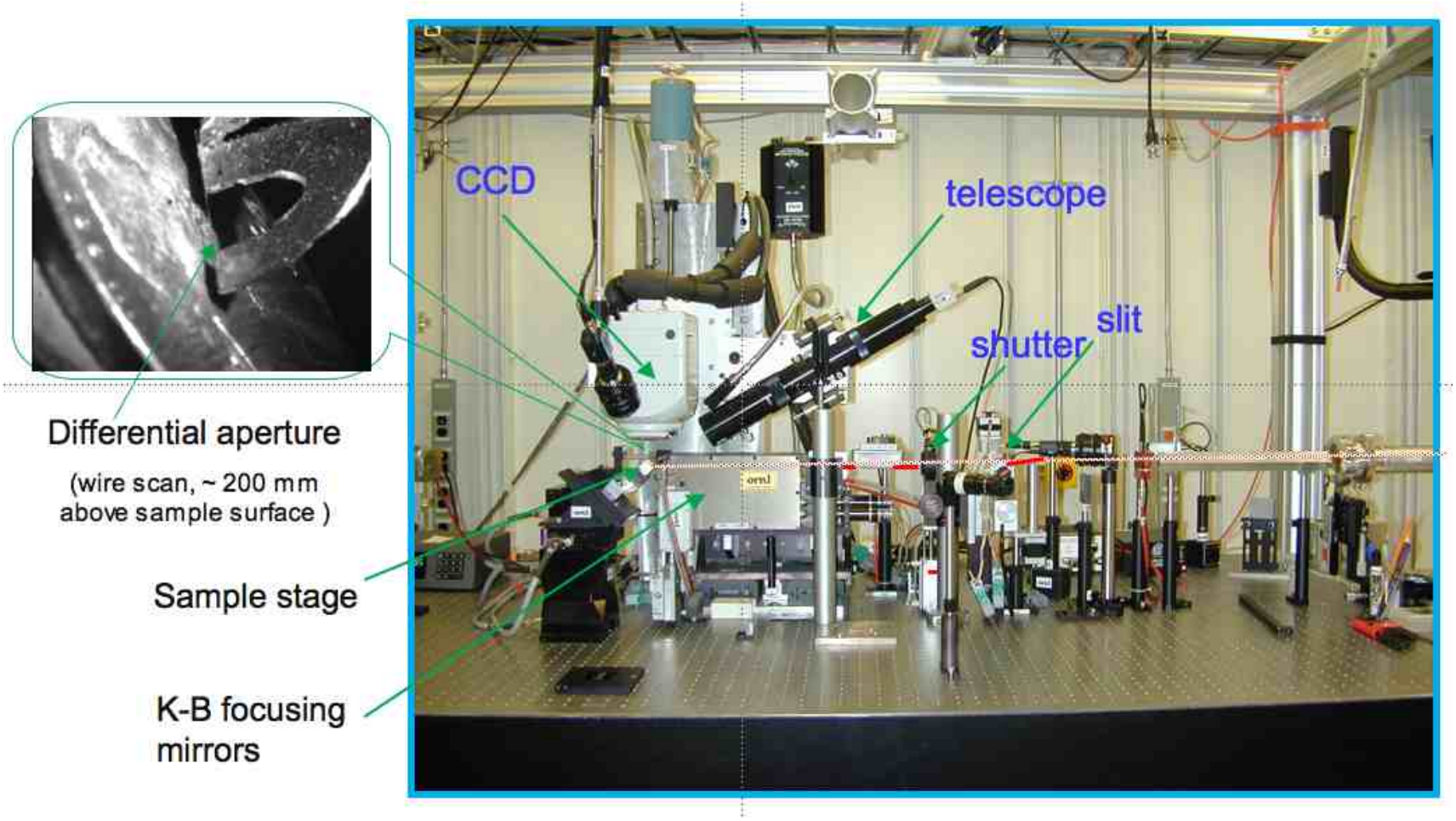

DAXM illuminates the 3D structure of aluminum

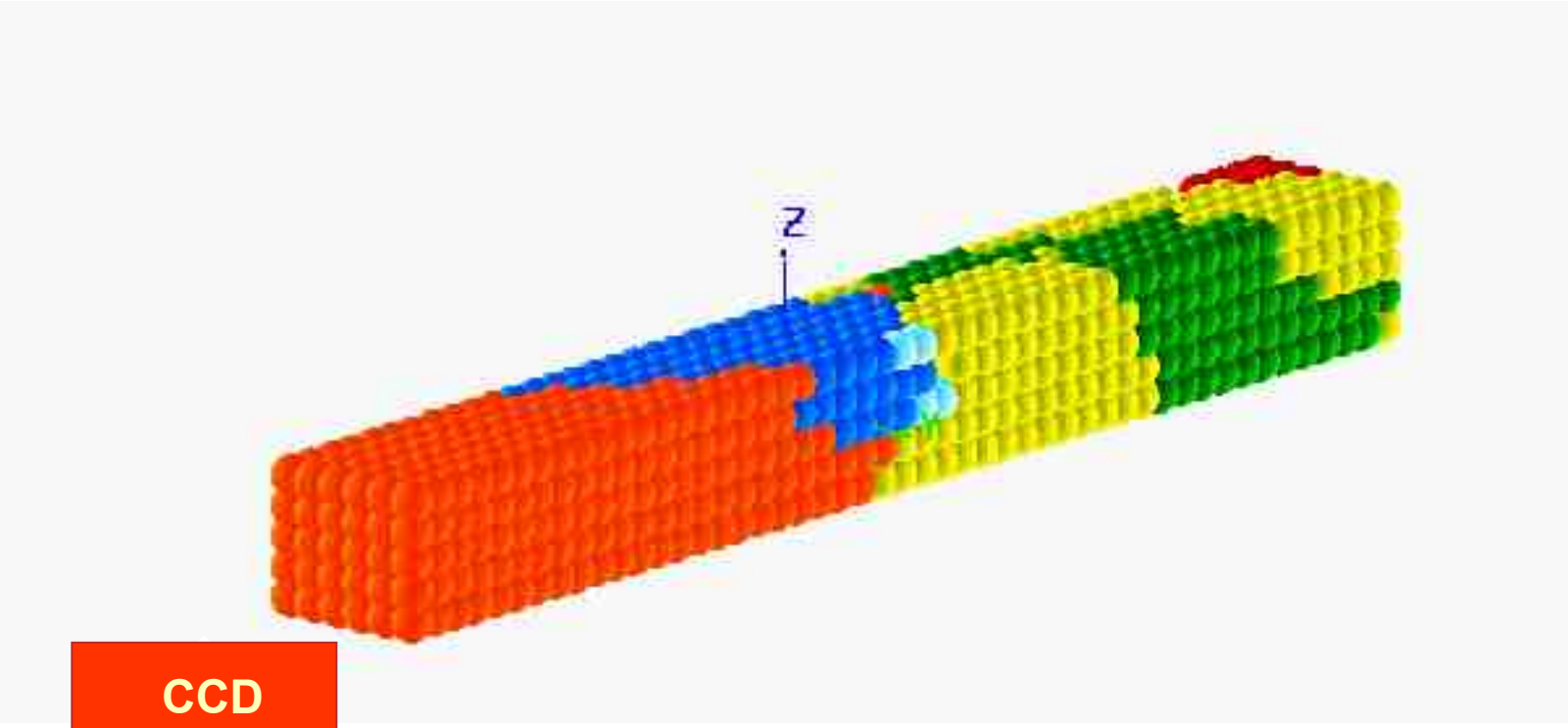

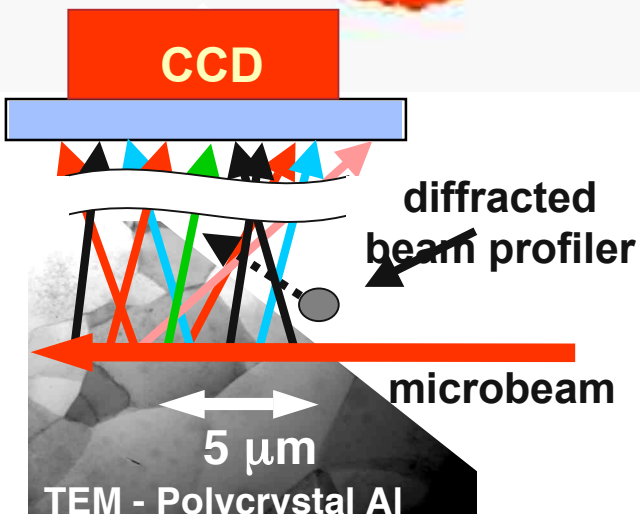

- Intra- and inter-granular information
- Grain boundary morphology and type
- Misorientation axis/angle between grains
- 3D microtexture
- Grain size-distribution

W. Yang, *Micron* 35, 431 (2004)

Electromigration induces strain in polycrystalline conductors

- EM results in stresses and strains in conductors that can lead to voids, cracks, passivation, increased resistance …
- Bamboo-like grain structure (grain boundaries perpendicular to electron flow) is desirable for resistance to EM

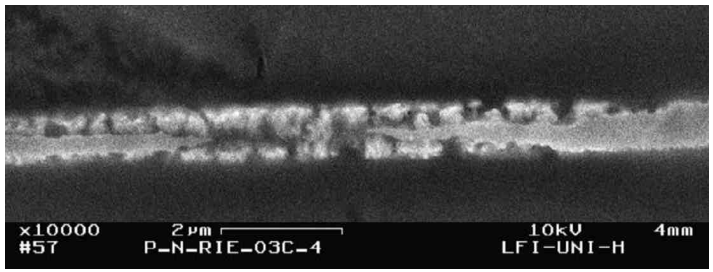

SEM image of a EM failure in an interconnect

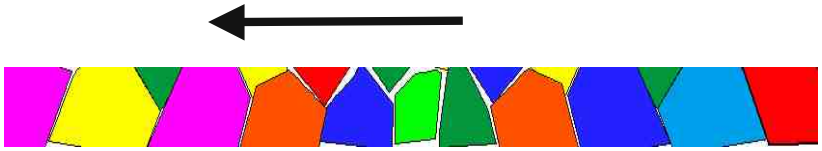

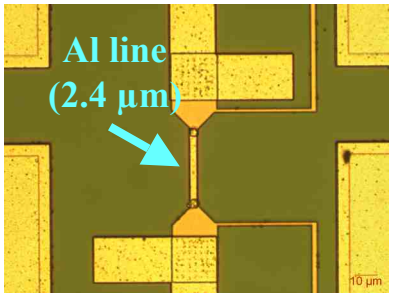

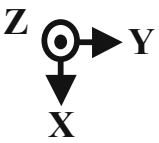

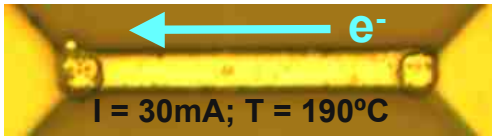

Current density: 1.54 ×10^6 A/cm^2

Before EM, elastic strain along the Al line was nearly uniform. During 18 hrs of EM, elastic strain gradients were formed along the line without significant resistance change.

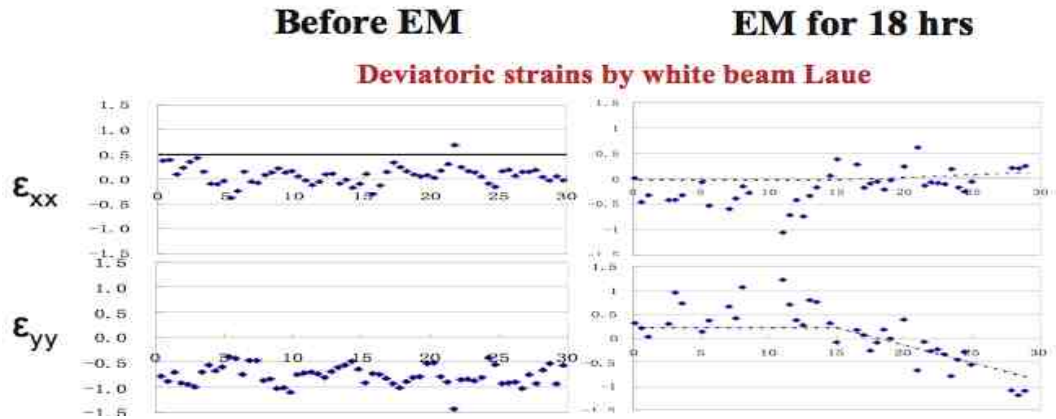

Coherent diffraction and holography: "Lensless" imaging

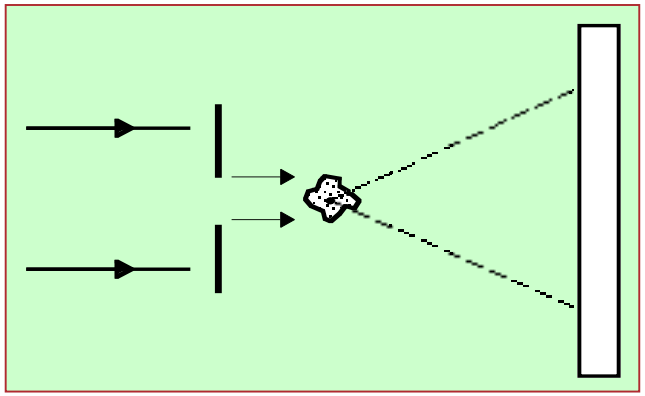

Coherent Diffraction

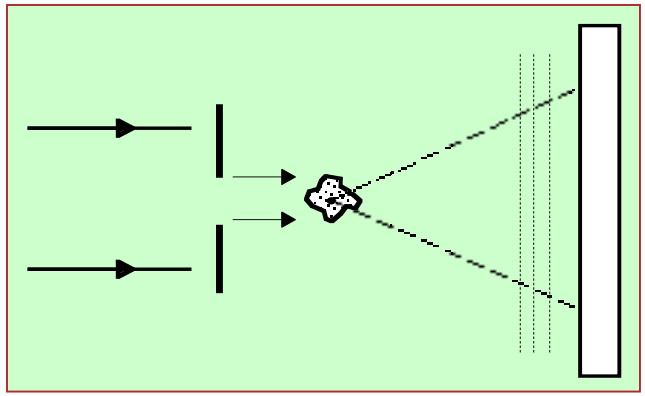

Holography

- **Object wave (diffraction) is detected directly**
- **Diffraction intensity corresponds to autocorrelation of object**

- **Coherent reference wave interferes with object wave to form hologram**
- **Hologram intensity corresponds to convolution of object and reference**

Resolution:	**transverse**	**~ λ/NA**
	longitudinal	**~ λ/(NA)^2**
Contrast:		**∝ |$f_1^2 + f_2^2$|**

X-ray scattering from a disordered sample

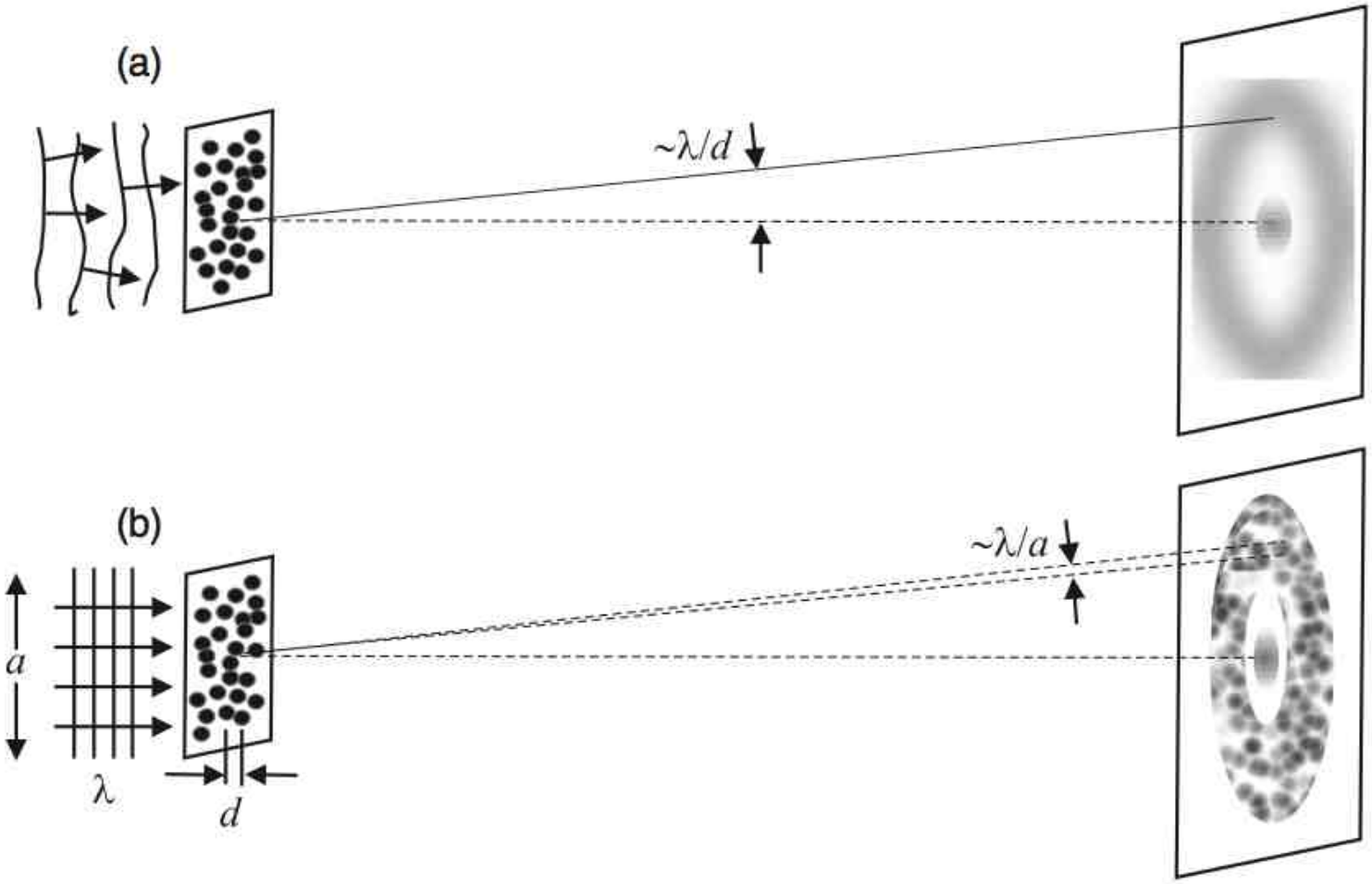

X-ray diffraction from a disordered medium with particle distance d and object size a.
(a) **Incoherent scattering**, giving rise to a continuous diffraction ring.
(b) **Coherent scattering**, resulting in a speckled diffraction ring.

F. van der Veen and F. Pfeiffer, J. Phys. Cond. Mater. 16, 5003 (2004)

Coherent diffractive imaging

Lensless method - resolution limited only by wavelength, signal

- Two-step process: record coherent diffraction patternm, recover object structure numerically (iterative phase retrieval)
- Sensitive to phase as well as absorption of the specimen
- Get 3D by tomographic methods; no depth of field limit
- But: must assume some *a priori* information to recover phase, e.g. known object extent or illumination profile

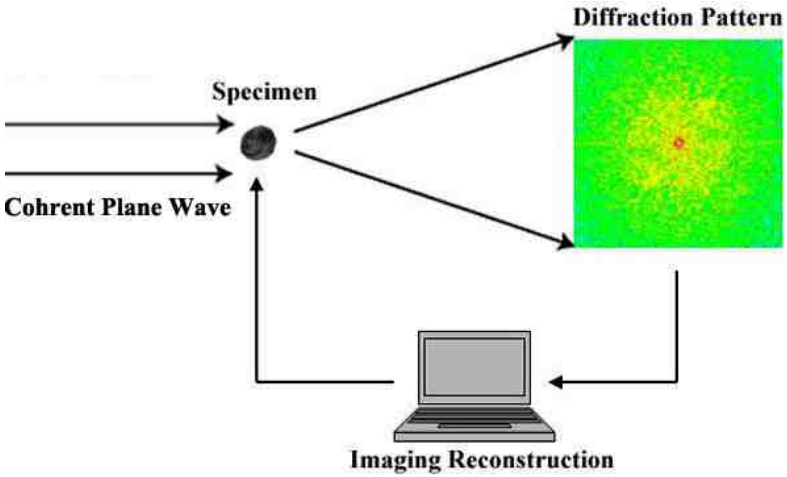

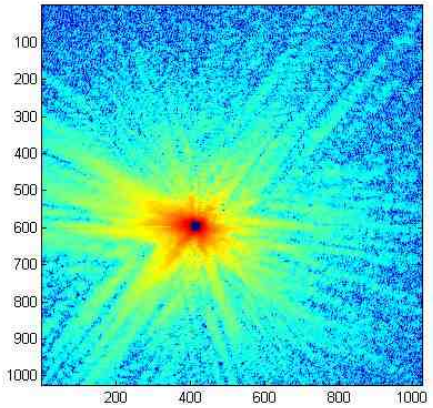

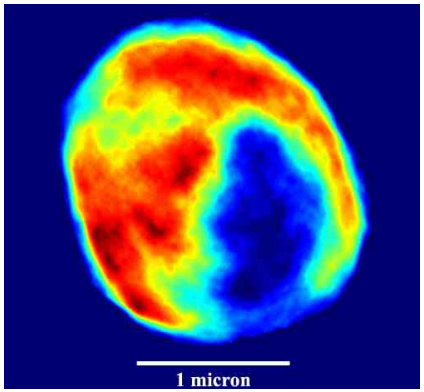

resolution ~ λ / angular size

J. Miao, Nature 400, 342 (1999)

Iterative phase retrieval

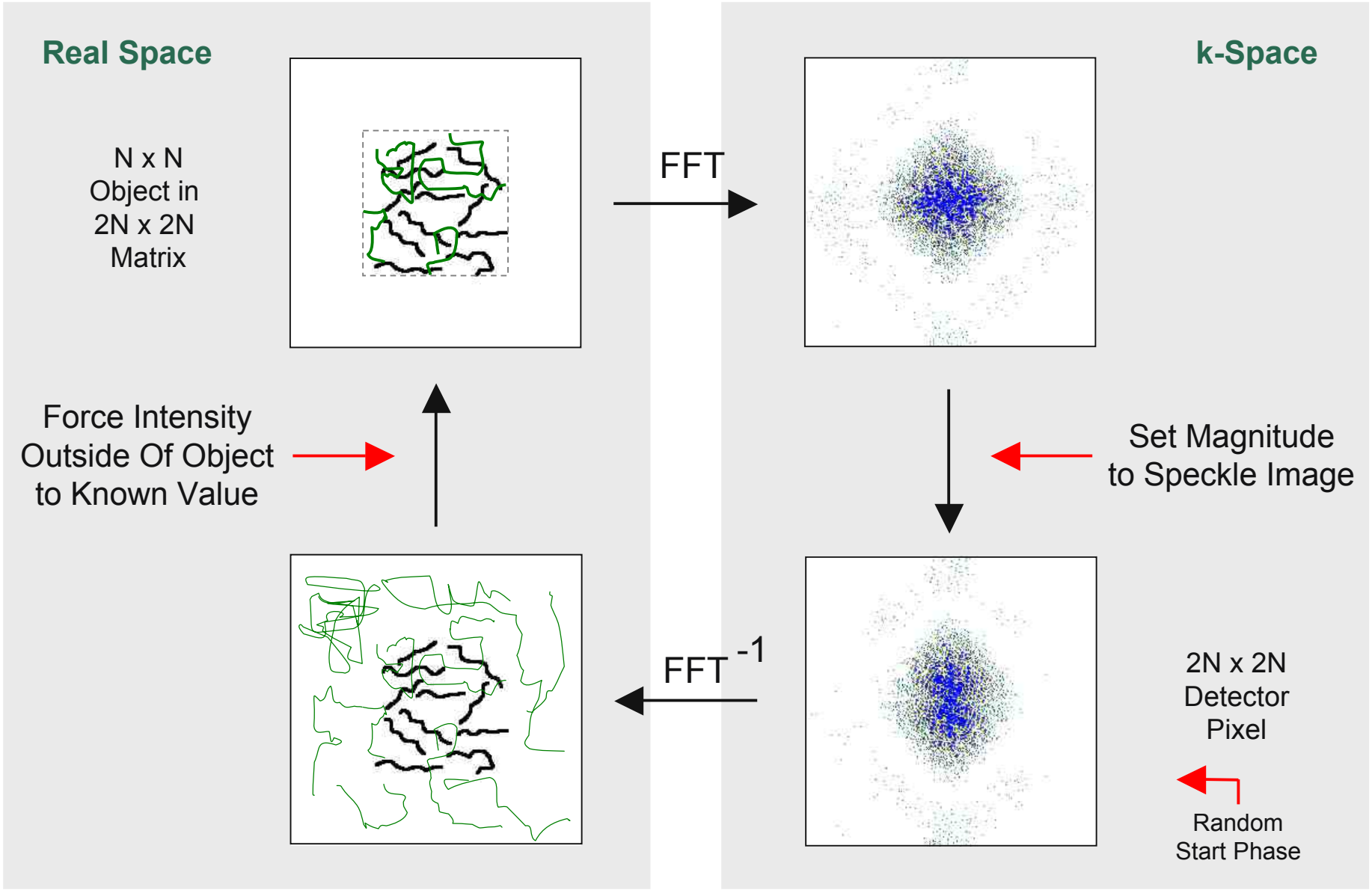

R. Gerchberg and W. Saxton, *Optik* 35, 237 (1972); J.R. Fienup, *Appl. Opt.* 21, 2758 (1982)

Freeze dried yeast cell imaged by coherent x-ray diffraction

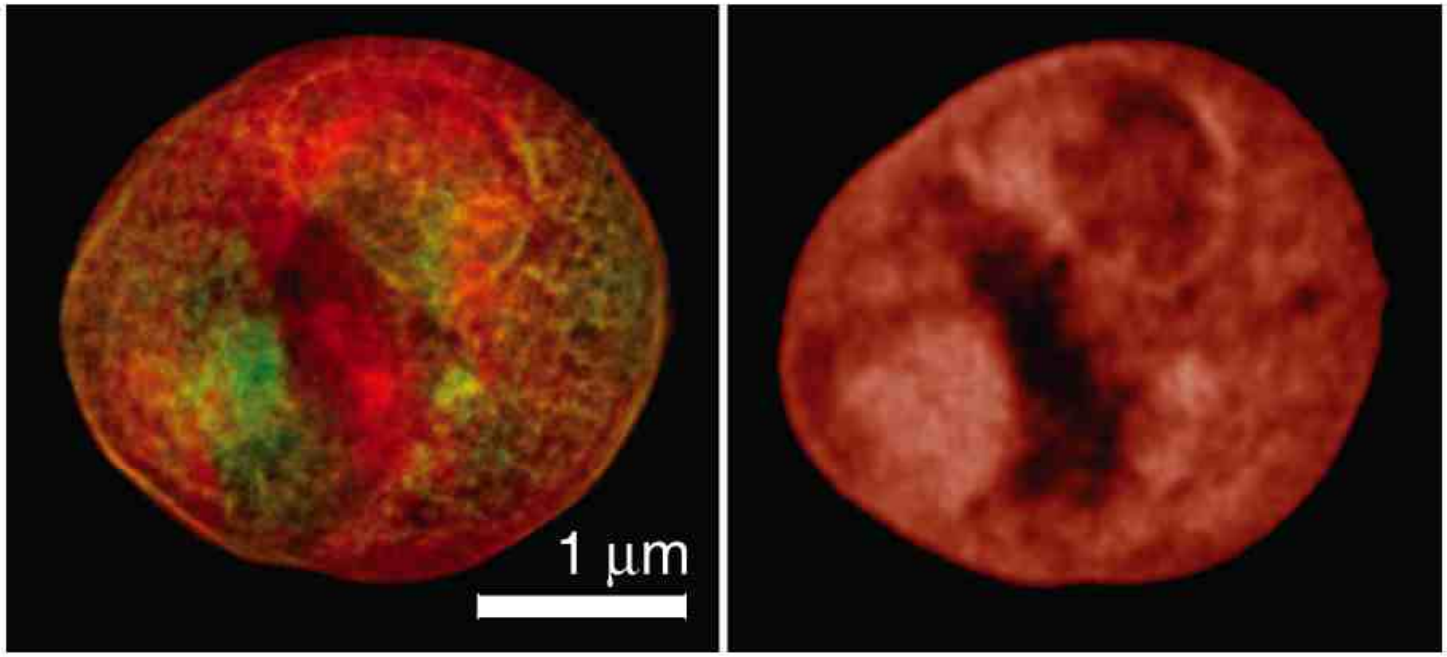

Diffraction reconstruction (data taken at 750 eV; absorption as brightness, phase as hue).

Stony Brook/NSLS STXM image with 45 nm Rayleigh resolution zone plate at 520 eV (absorption as brightness)

D. Shapiro, *PNAS* 102, 15343 (2005)

Buried structures can be probed with element specificity

In contrast to weak segregation theory, Bi is locally concentrated in Bi-doped Si crystals

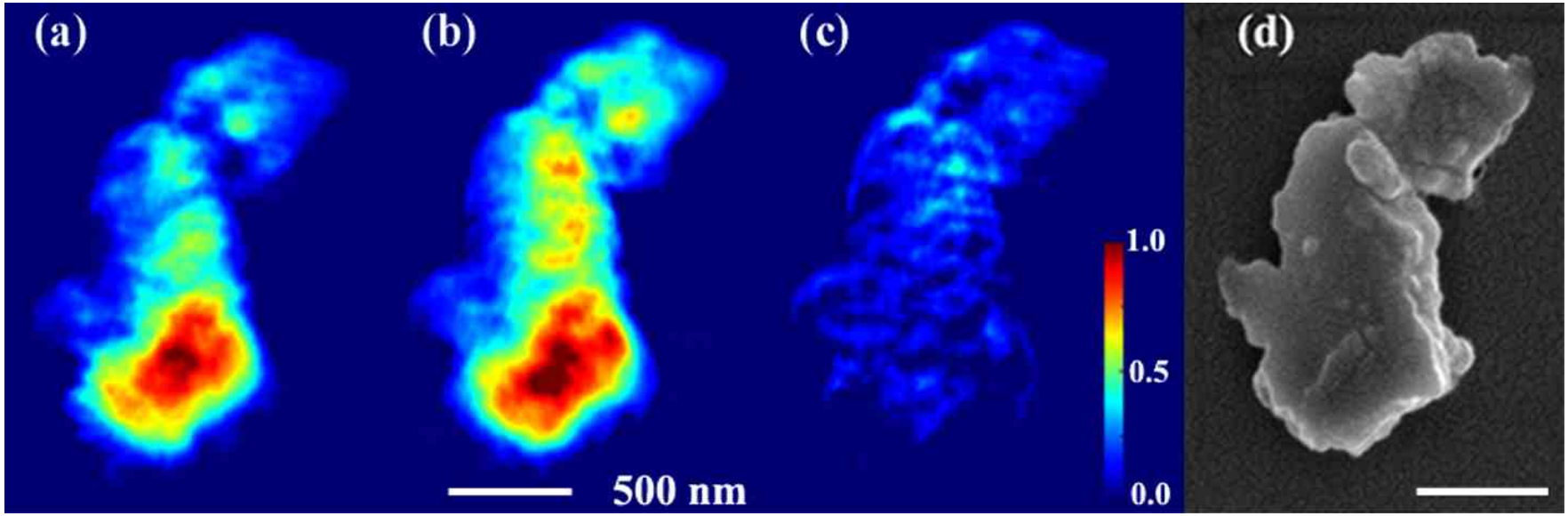

(a) Image below Bi M5 edge (2550 eV)
(b) Image above the Bi M5 edge (2595 eV)
(c) Difference
(d) SEM image

C. Song, PRL 100, 025504 (2008)

CDI setup at APS beamline 2-ID-B (1-4 keV)

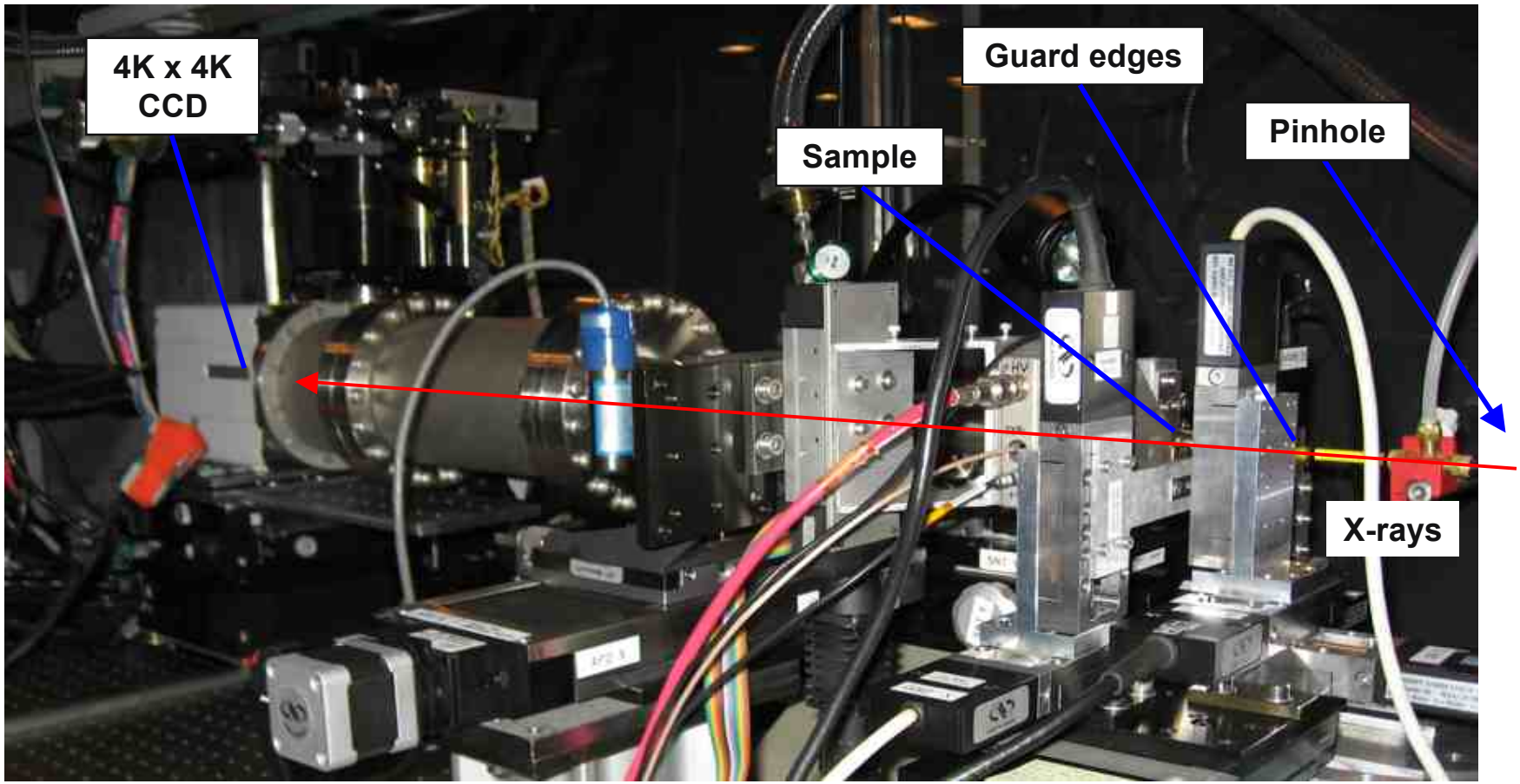

Diffraction microscopy in 3D

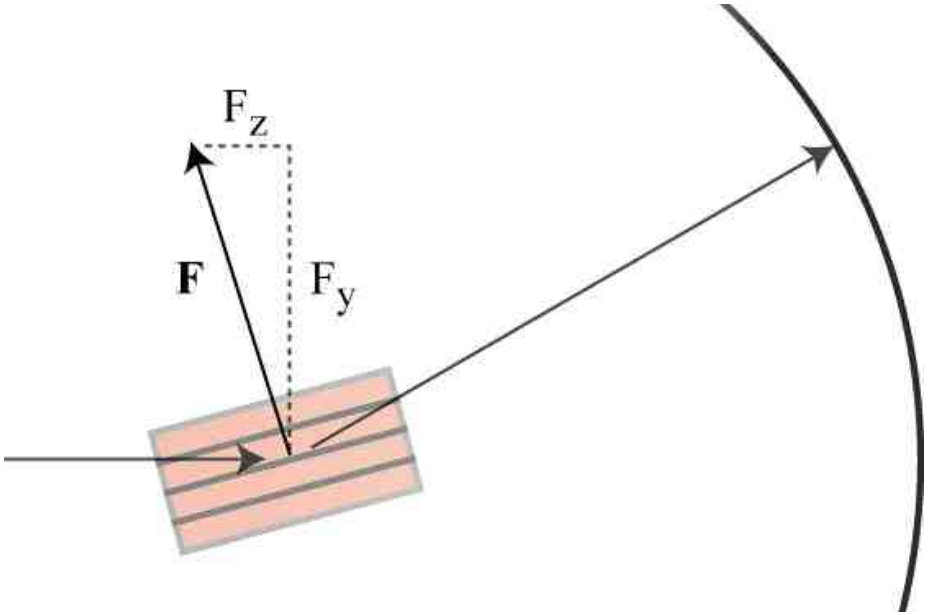

Bragg gratings that diffract to a certain angle represent a specific transverse and longitudinal periodicity (Ewald sphere)

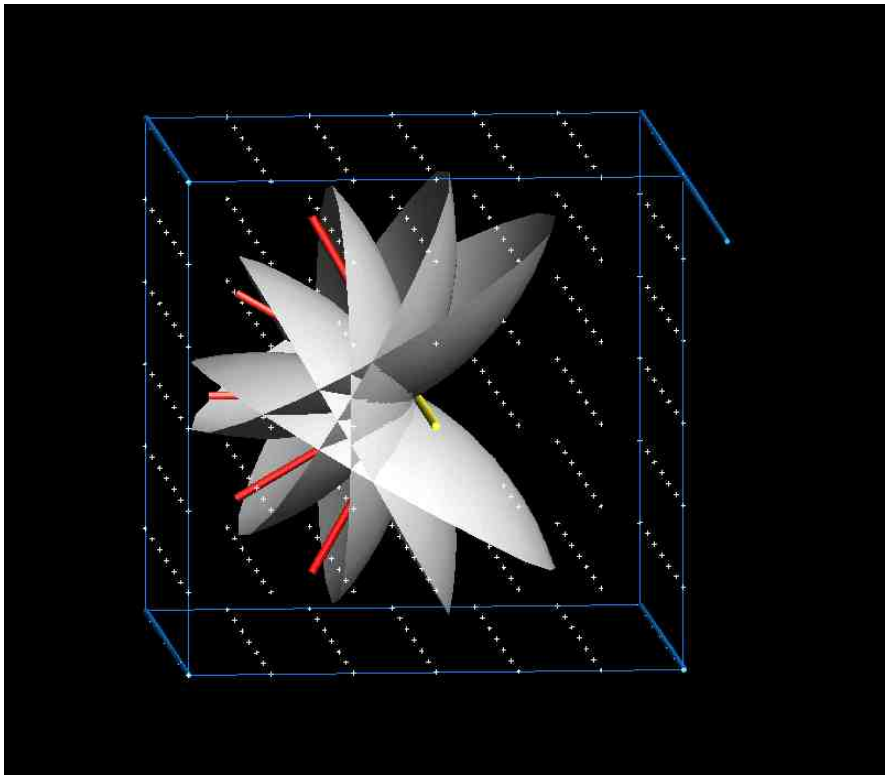

Data collection over a series of rotations about an axis fills in 3D Fourier space for phasing

3D coherent diffraction imaging

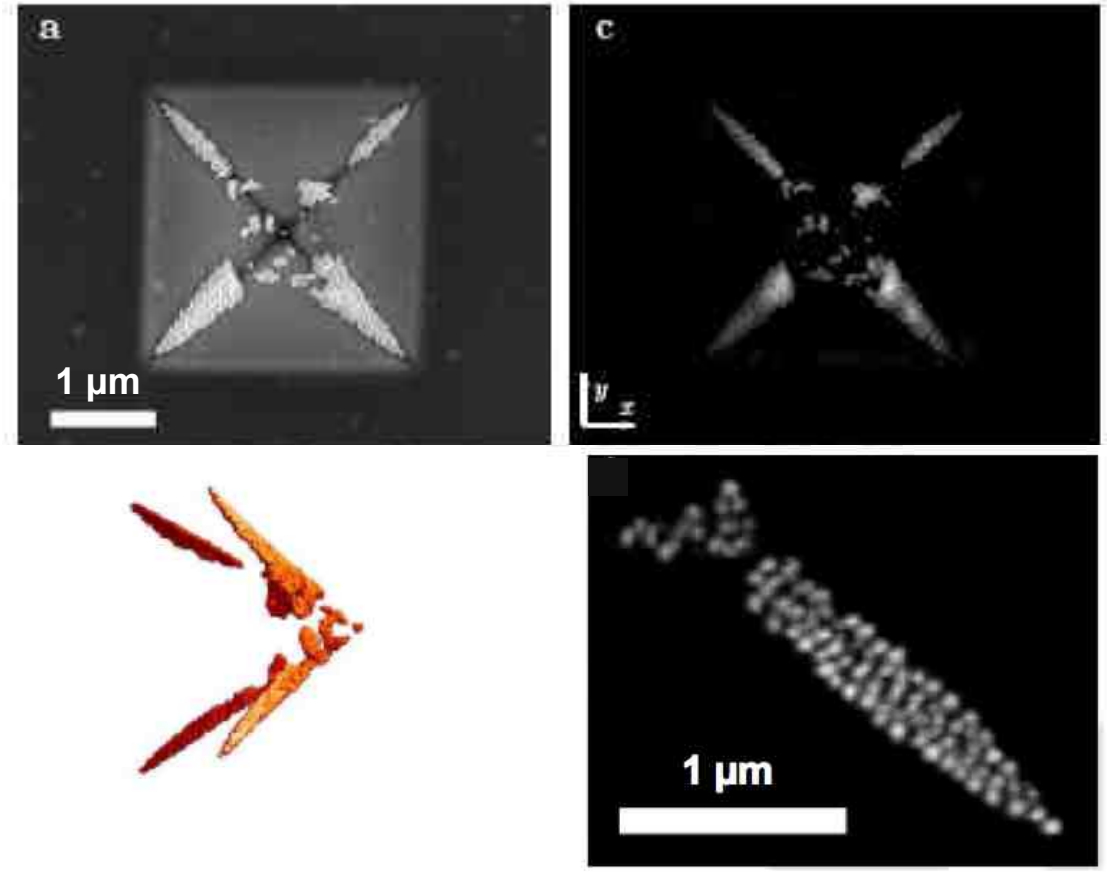

(a) SEM of pyramidal indentation in a 100-nm Si_3N_4 membrane lined with 50-nm Au spheres. (b) 3D image reconstructed from 123 diffraction projections spanning -57° to +66°, using reality and positivity constraints. (c) Large DOF projection. (d) Enlarged region of (c).

H. Chapman, JOSA A23, 1179 (2006)

3D experiments are beginning to yield fruit …

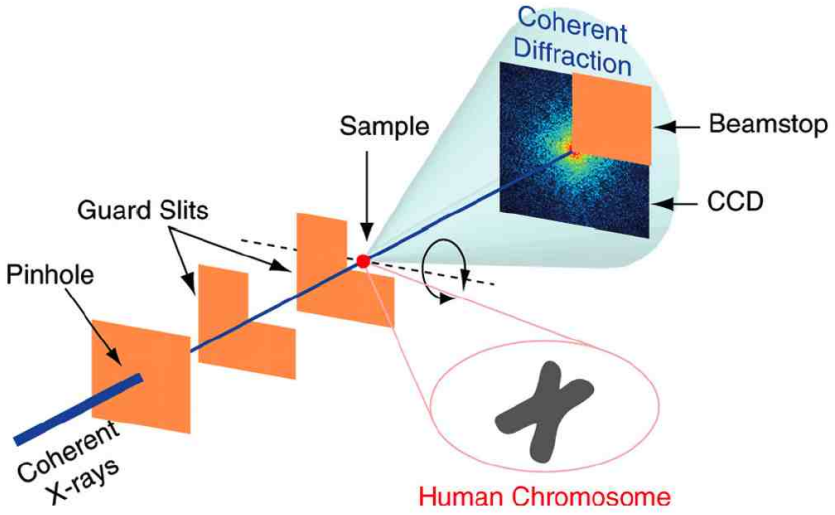

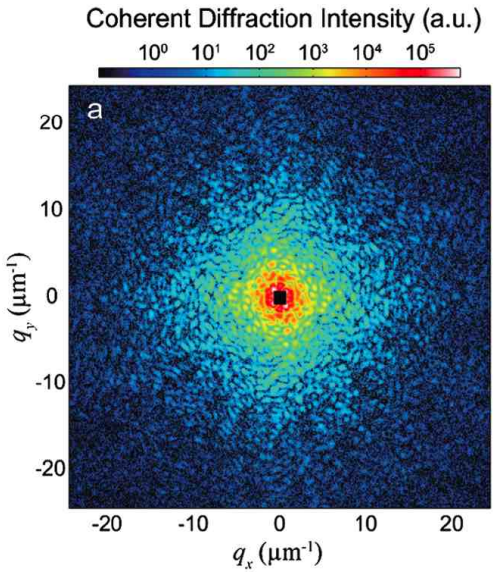

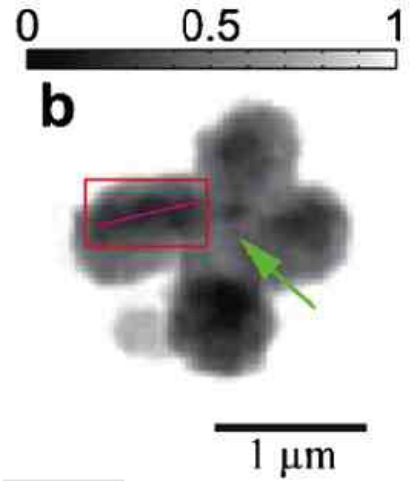

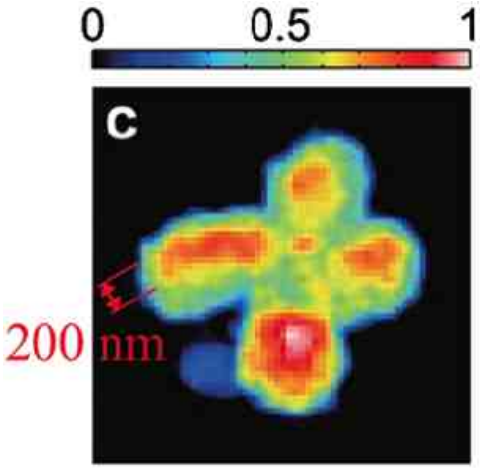

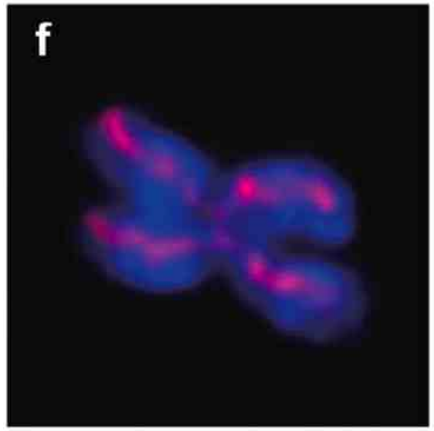

Y. Nishino, PRL 102, 018101 (2009)

Curved object illumination aids unique phase recovery

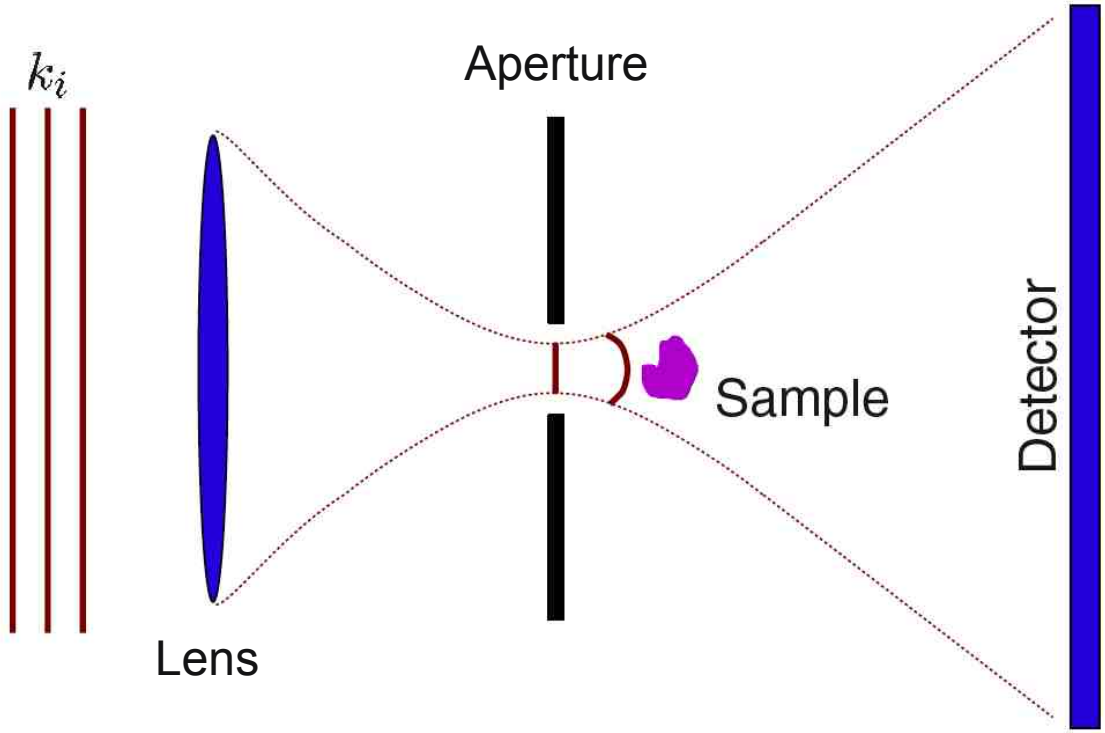

- Lens illuminates object with curved wavefront, defines field of view
- Object illumination is reconstructed by back-propagation, used to retrieve phase of object wave by iterative methods

K. Nugent, PRL 91, 203902 (2003)

... and converges faster

Original

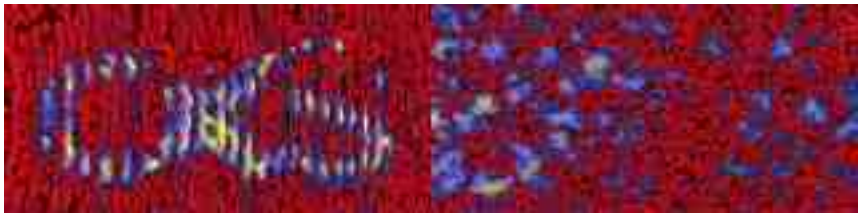

curved beam illumination

plane wave illumination

Fresnel diffraction

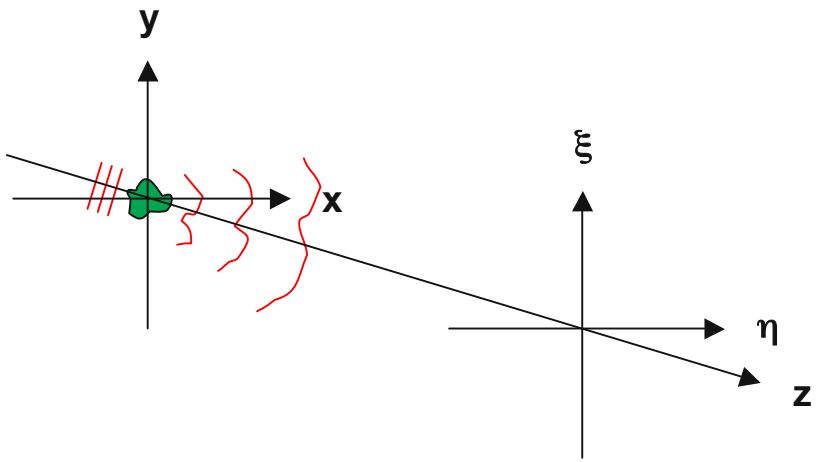

"object wave"

$$a(\xi,\eta) = \frac{e^{ikz}}{i\lambda z}\iint a(x,y)\; e^{\frac{ik}{2z}\left((x-\xi)^2+(y-\eta)^2\right)}\,dxdy$$

$$= \frac{e^{ikz}}{i\lambda z}\; e^{\frac{ik}{2z}\left(\xi^2+\eta^2\right)}\; \mathrm{FT}\left\{ e^{\frac{ik}{2z}\left(x^2+y^2\right)} a(x,y) \right\}$$

Fresnel coherent diffraction imaging of a gold test pattern

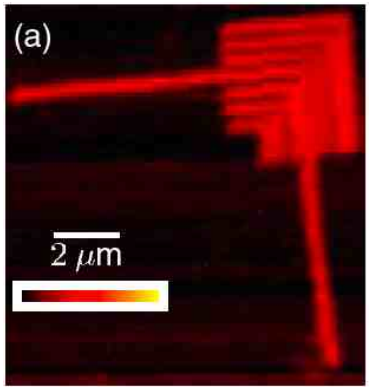

STXM image (1.8 keV)

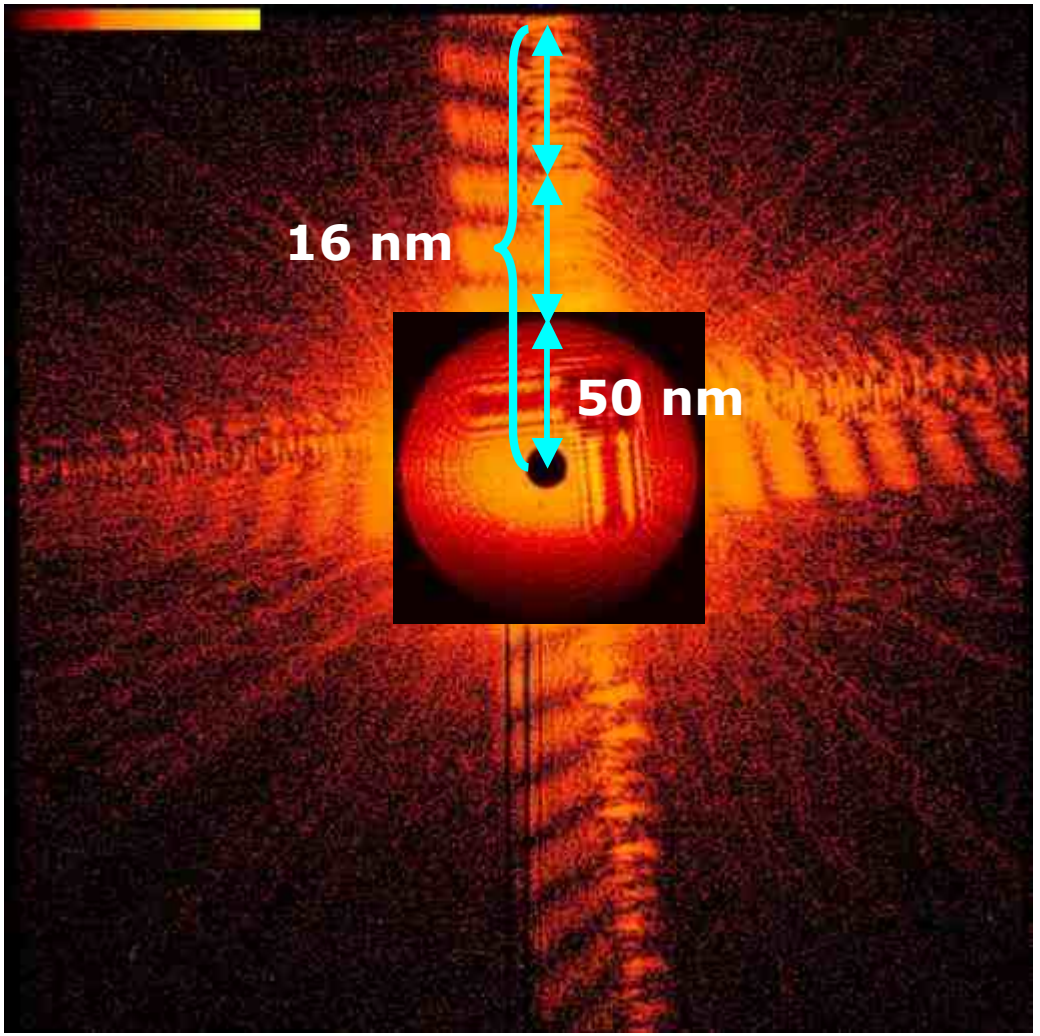

Images reconstructed by FCDI

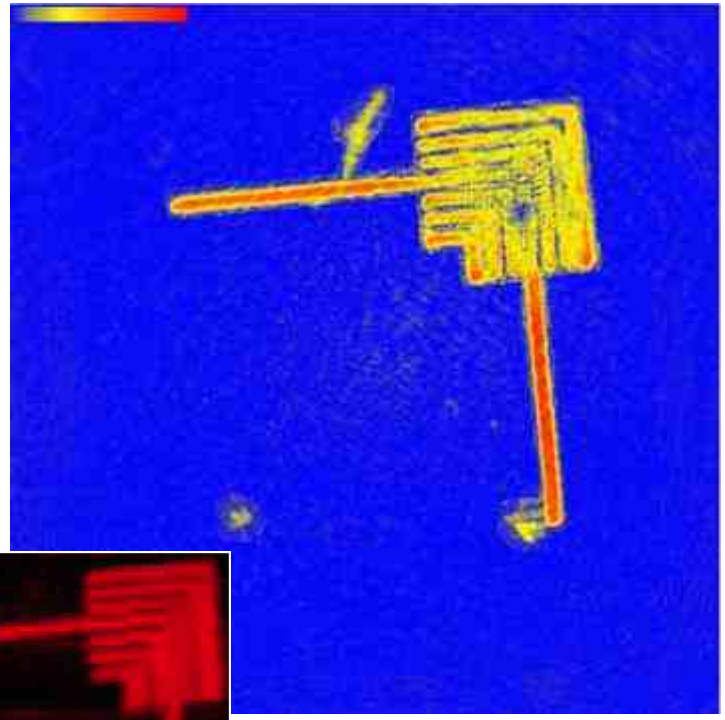

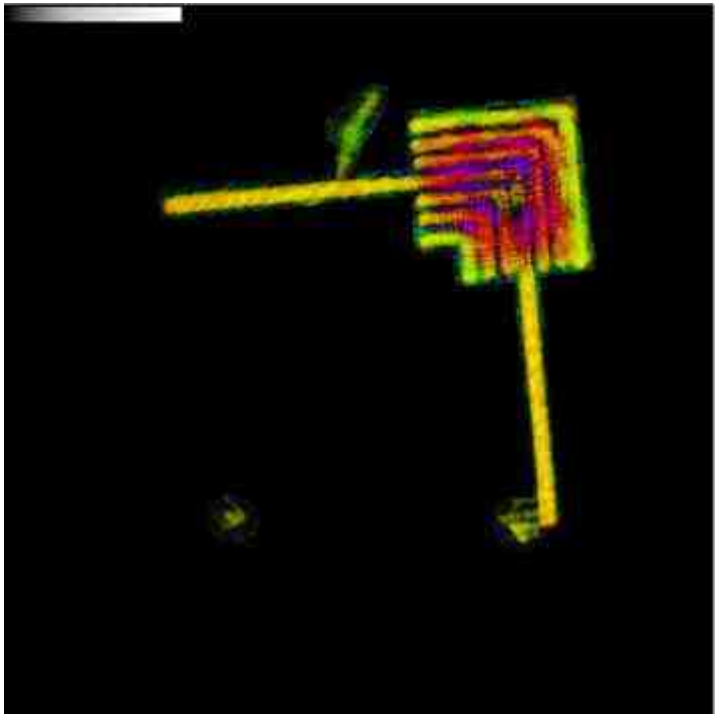

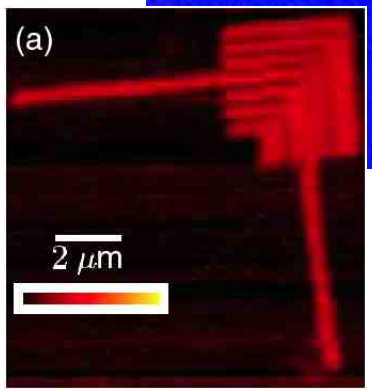

Phase

Magnitude with color-encoded phase

STXM image (1.8 keV)

G. Williams, PRL 97, 022506 (2006)

"Keyhole" FCDI

Use reconstructed illumination profile to determine support in extended sample

H. Quiney,
Nature Physics 2, 101 (2006)

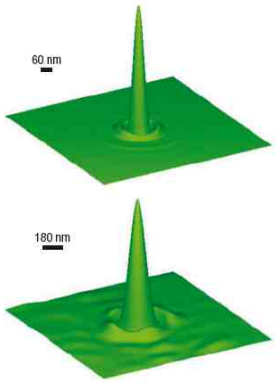

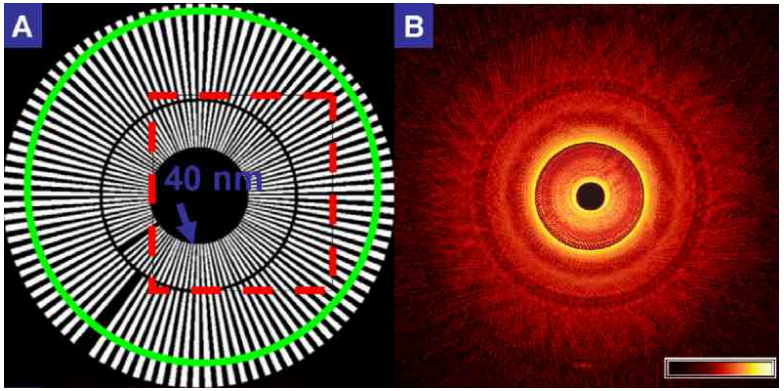

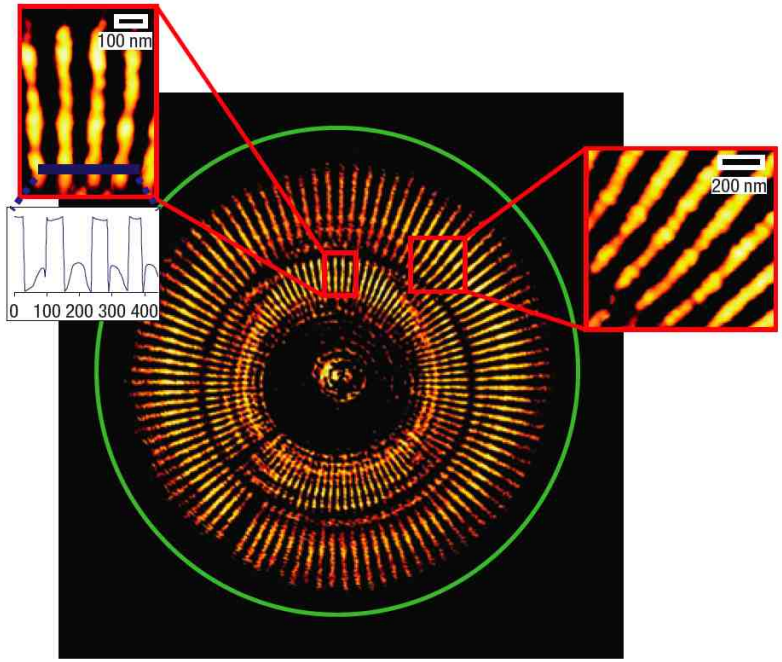

Ability to study extended samples is essential for many real-world problems!

B. Abbey, Nature Physics 4, 394 (2008)

"Fuse bay" structure

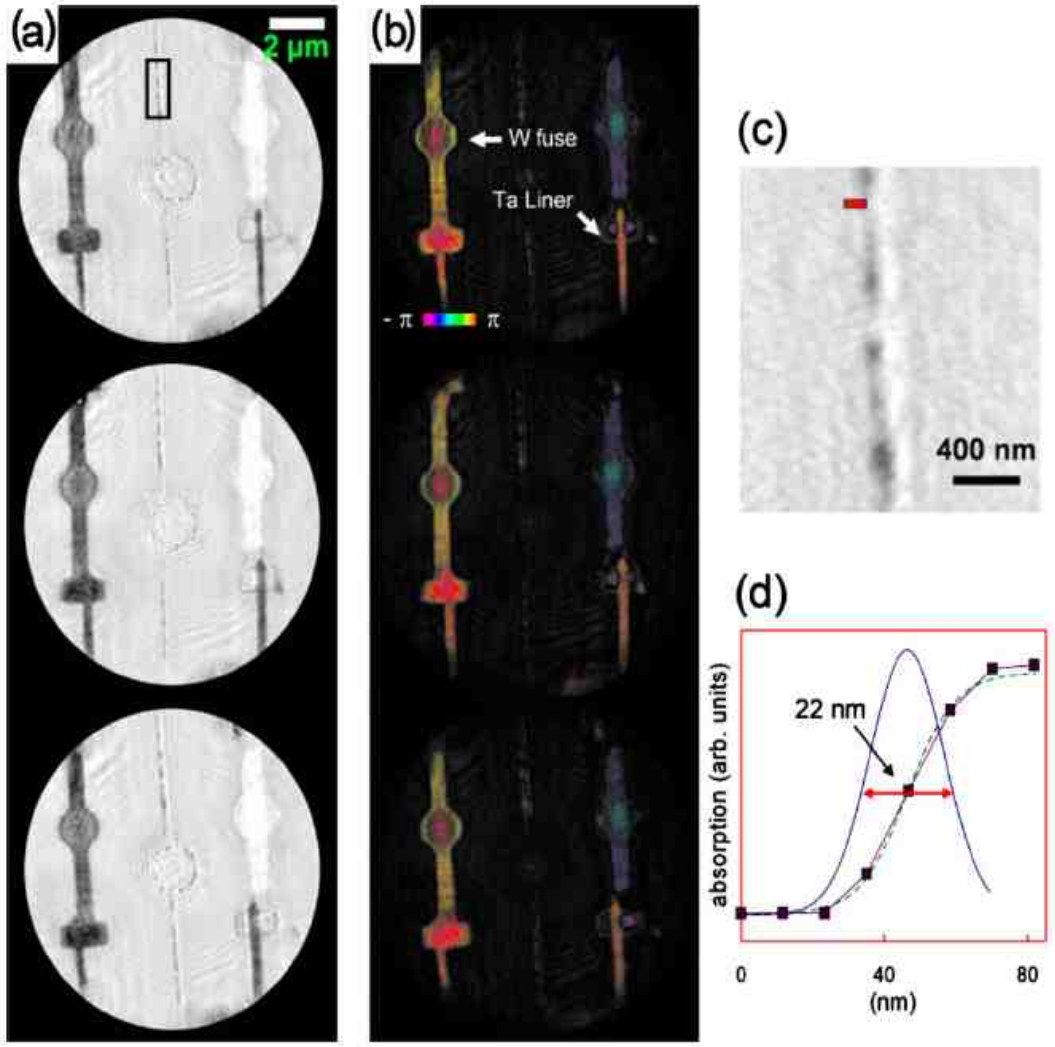

B. Abbey, APL 93, 214101 (2008)

CDI accesses earliest stages of dealloying (Ag-Au alloy)

- Pores and ligaments begin to form at the ~5 nm scale
- Further dealloying (but not annealing) results in 10 - 50 nm pores

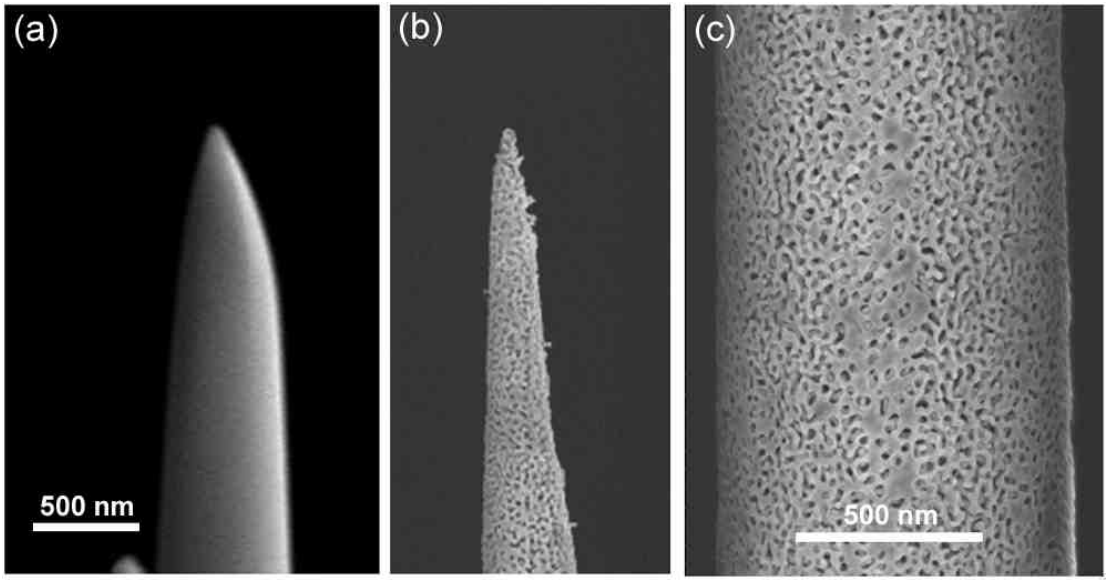

Scanning electron micrographs of (a) np-Au specimen before dealloying and (b,c) another specimen after dealloying

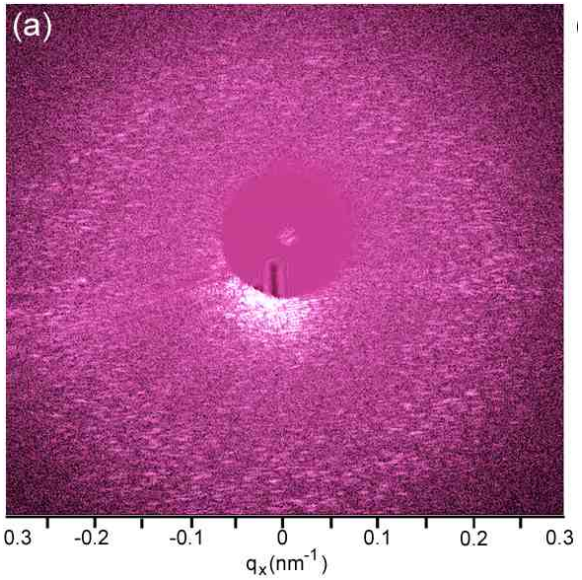

Fresnel coherent difraction pattern from dealloyed sample (2.185 keV)

X-ray phase gives quantitative thickness, density

- ***Goal: extract pore radii of curvature, local density, and ductility; correlate with SEM (surface) data***
- Full 3D dataset was recorded, reconstruction is underway

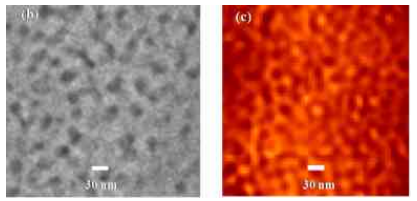

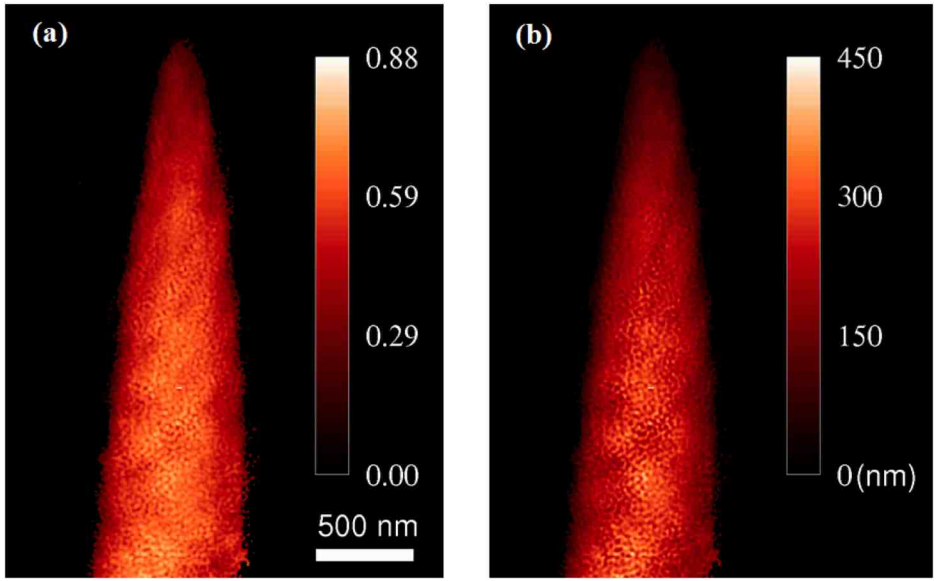

Reconstructed absorption coefficient and projected thickness obtained from reconstructed phase of the exit surface wave

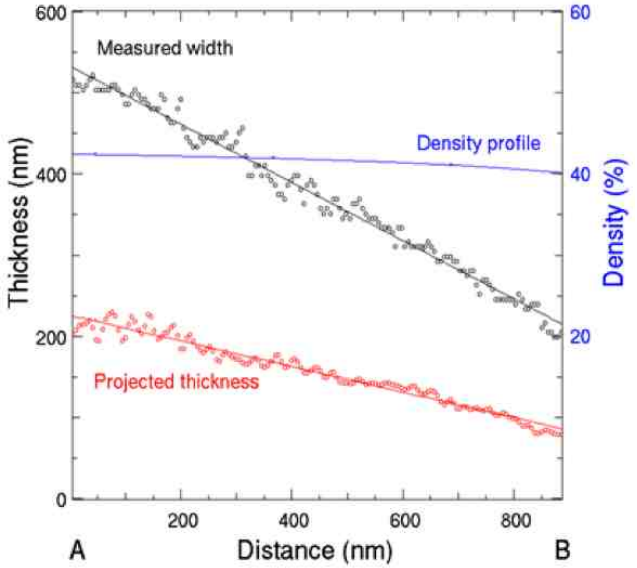

Measured width (0° view), projected thickness (90° view), and density as a function of position within sample

S. Kim (SACLA), et al., in preparation

Alternative approach: ptychography

R. Hegerl et al., Phys. Chemie 74, 1148 (1970)

H. Faulkner and J. Rodenburg, PRL 93, 023903 (2004)

J. Rodenburg et al., Phys. Rev. Lett. 98, 034801 (2007)

P. Thibault et al., Science 321, 379 (2008)

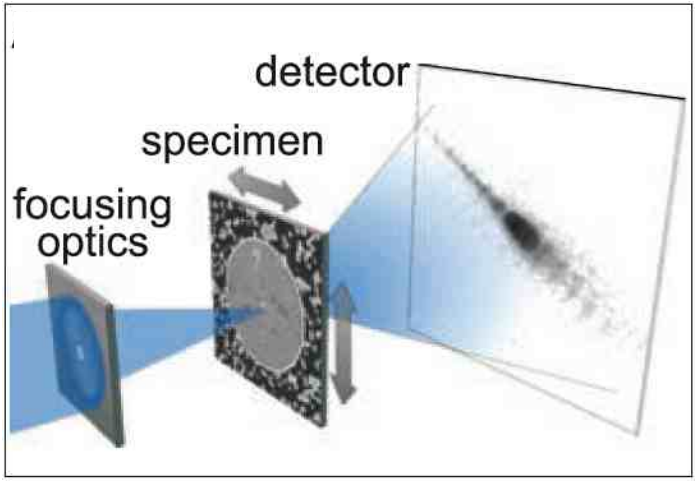

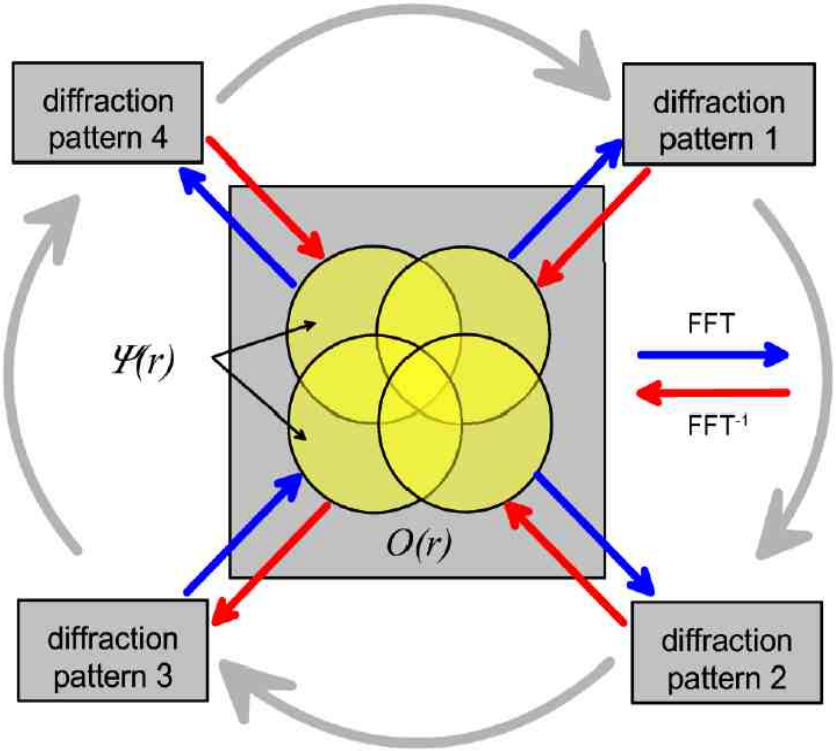

Does your iPad hold enough?

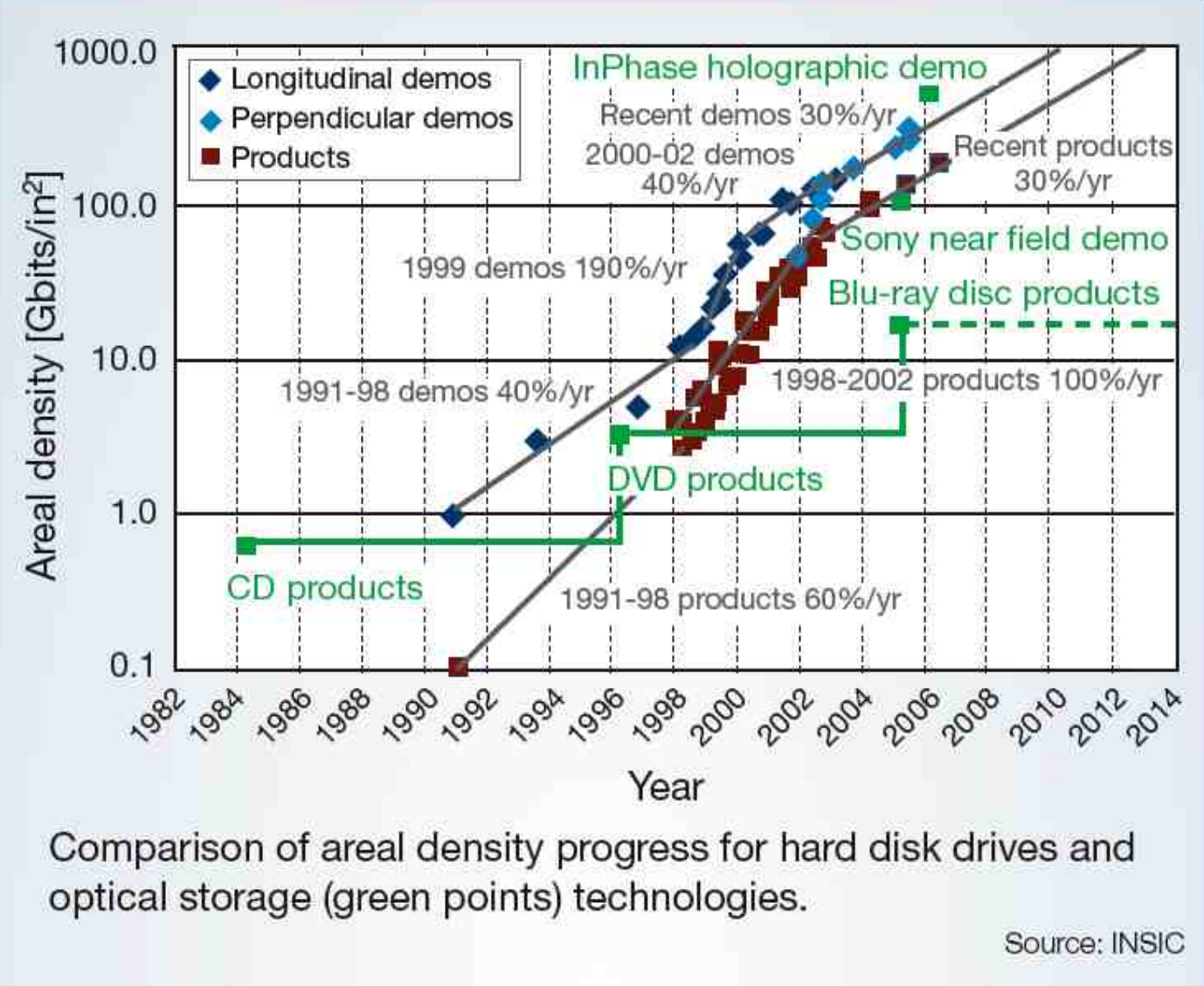

GdFe multilayers: a model system

- Fabricated by sputtering; can be nano-patterned lithographically
- Perpendicular anisotropy spontaneously forms "worm" domains with antiparallel out-of-plane magnetization
- Artificial ferrimagnets with strong coupling at domain interfaces

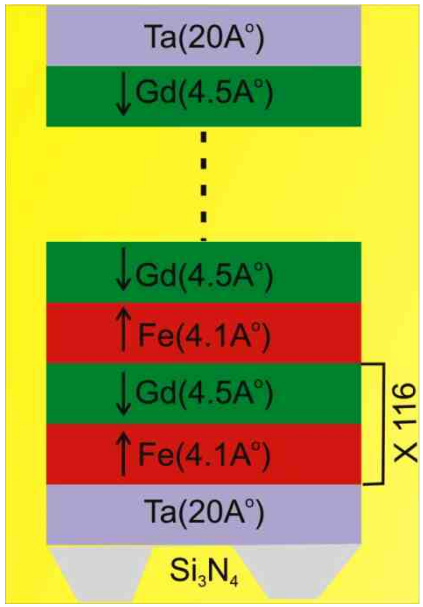

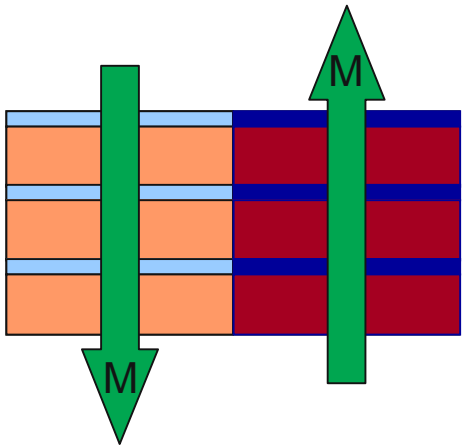

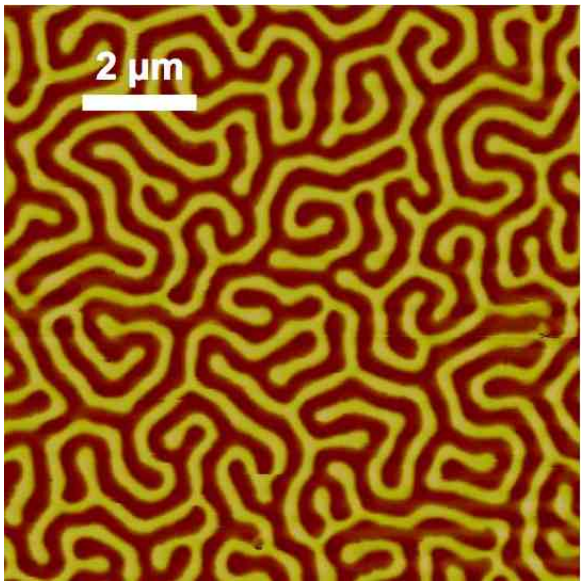

Magnetic force micrograph of 200 nm thick GdFe multilayer (courtesy E. Fullerton, UCSD)

Resonant x-ray scattering

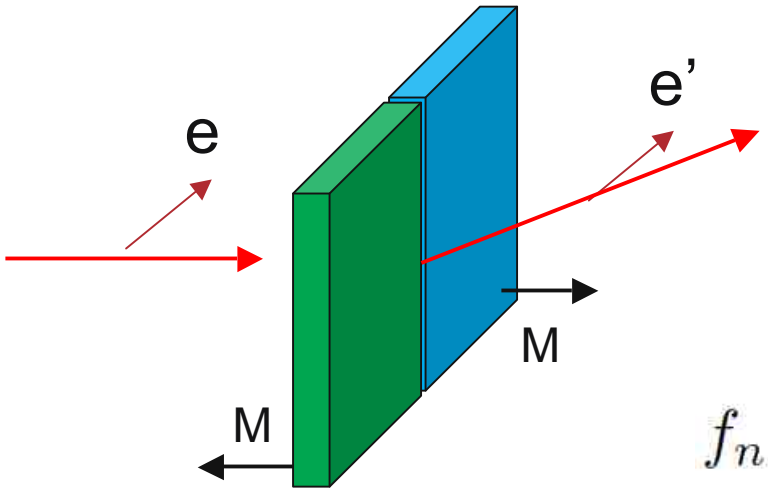

$$f_n \approx f^0_{nonres} + f^{magn}_{nonres} + f' + if''$$

~0 in this geometry

charge magnetic circular magnetic linear

$$f_{res} = \mathbf{e}' \cdot \mathbf{e}\, F_n^c - i\,(\mathbf{e}' \times \mathbf{e}) \cdot \mathbf{M}_n\, F_n^{m1} + (\mathbf{e}' \cdot \mathbf{M}_n)(\mathbf{e} \cdot \mathbf{M}_n)\, F_n^{m2}$$

$$I \propto \left| \sum_n \exp(i\mathbf{q} \cdot \mathbf{r}_n) f_n \right|^2$$

J.P. Hannon, PRL 61, 1245 (1988)

Magnetic domain structure can be visualized in-situ *with resonant x-ray coherent diffraction*

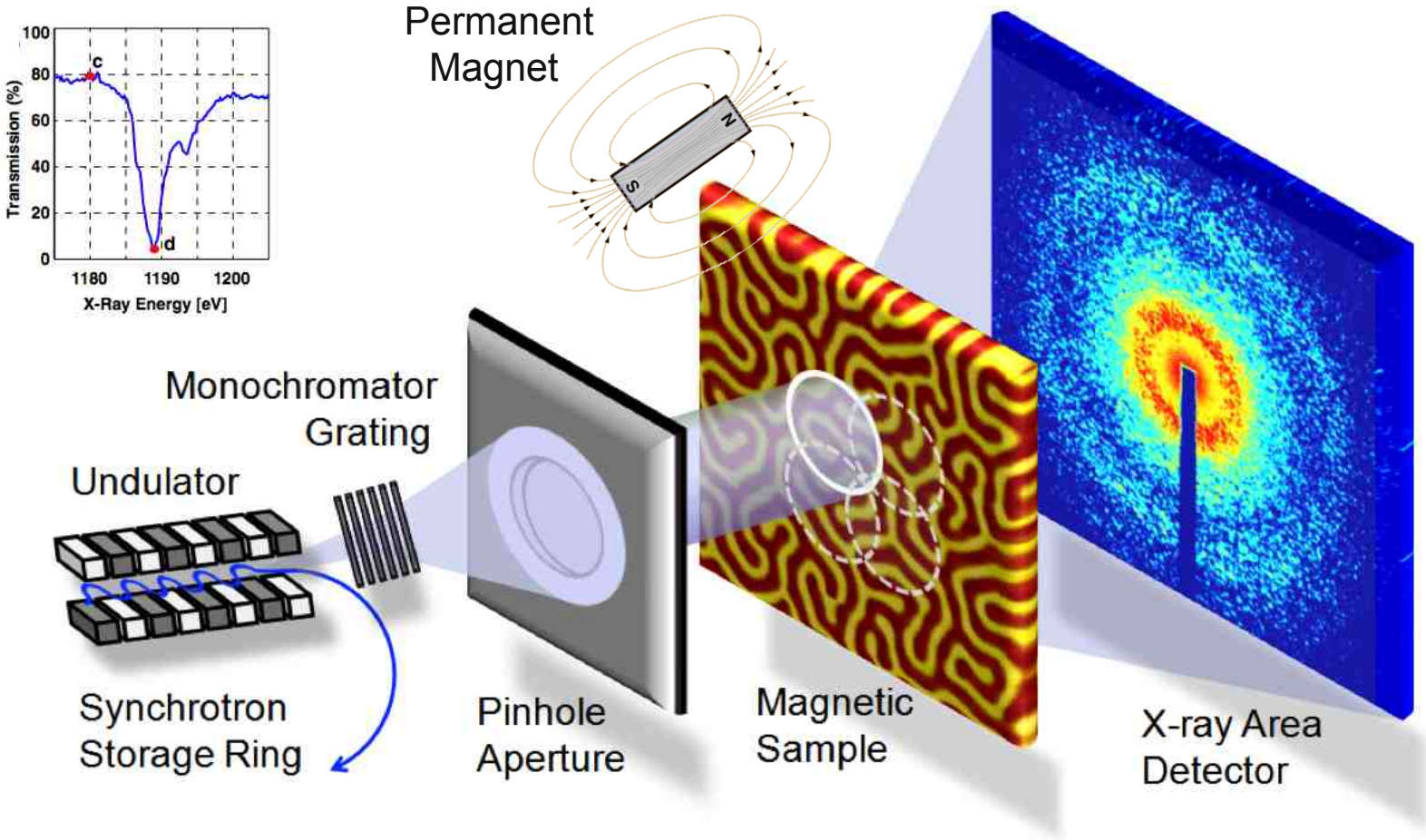

Resonant scattering vs. photon energy

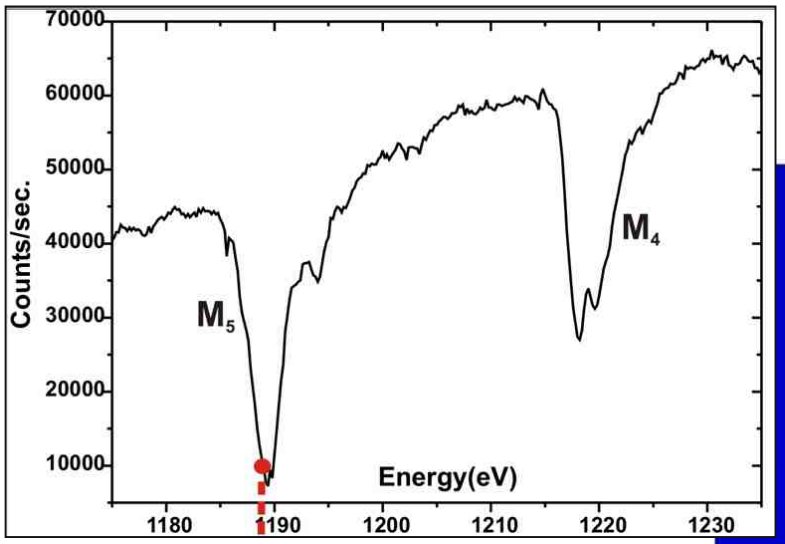

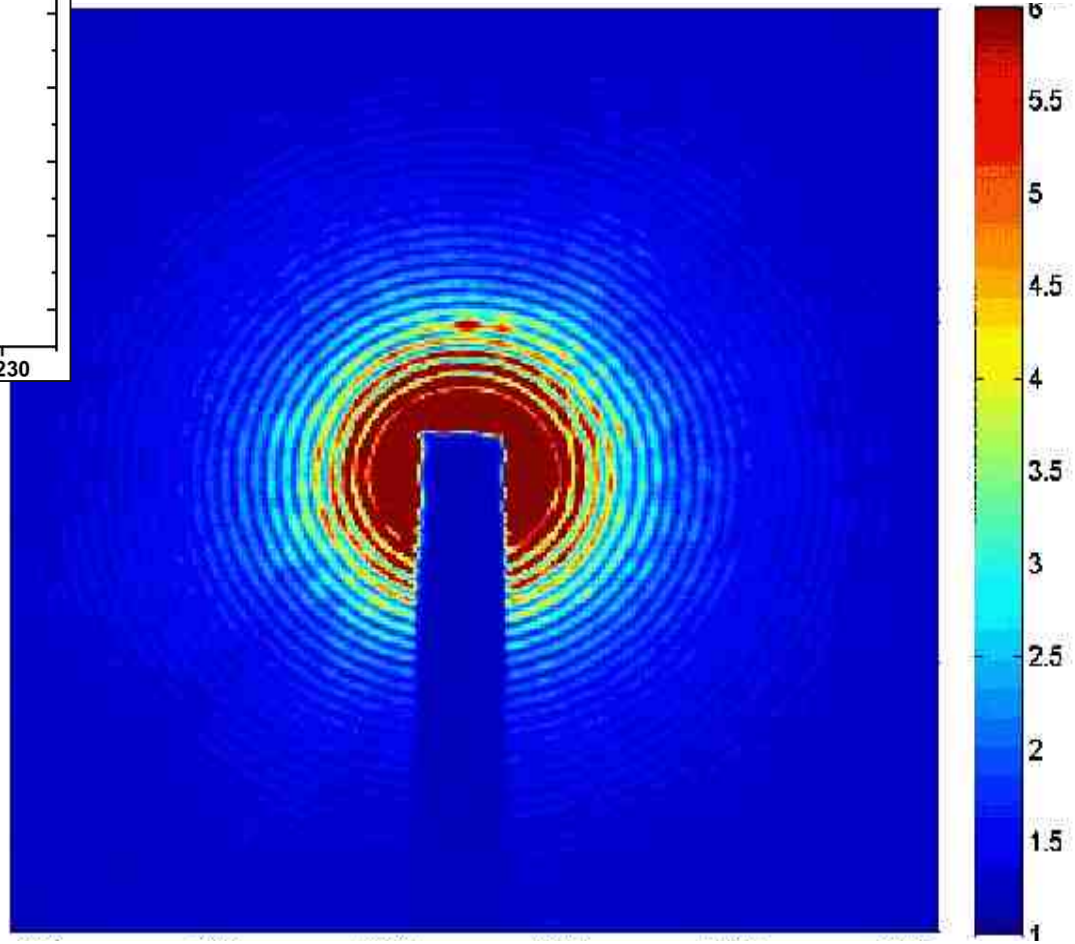

Many domain configurations are possible, depending on the magnetic history of the system

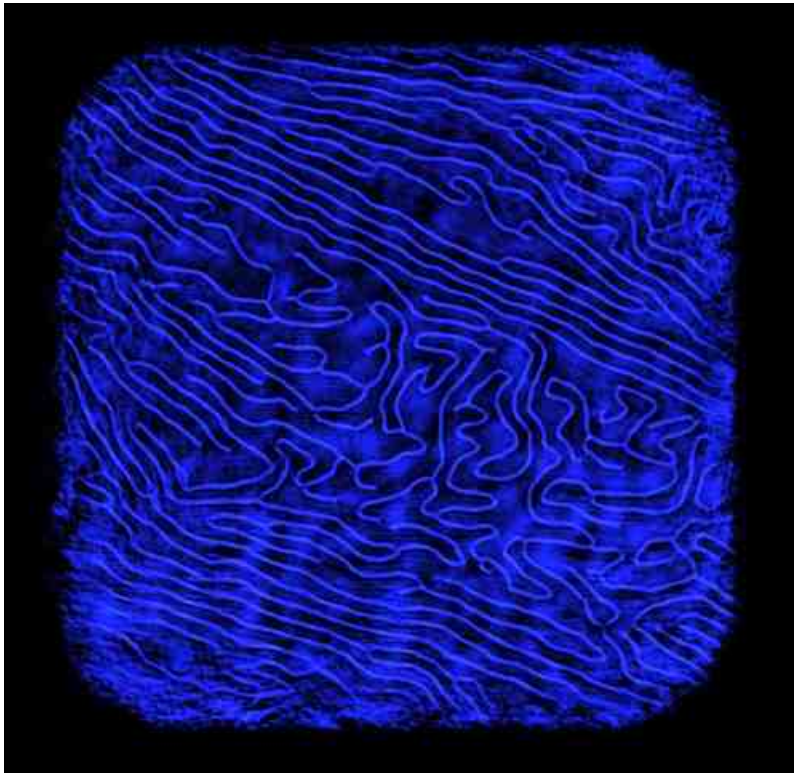

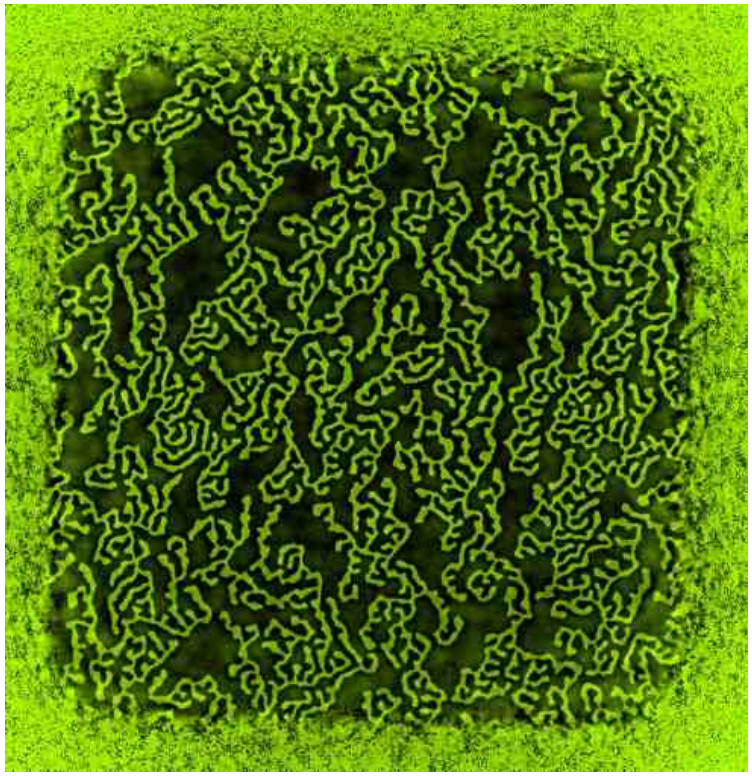

Decreasing field

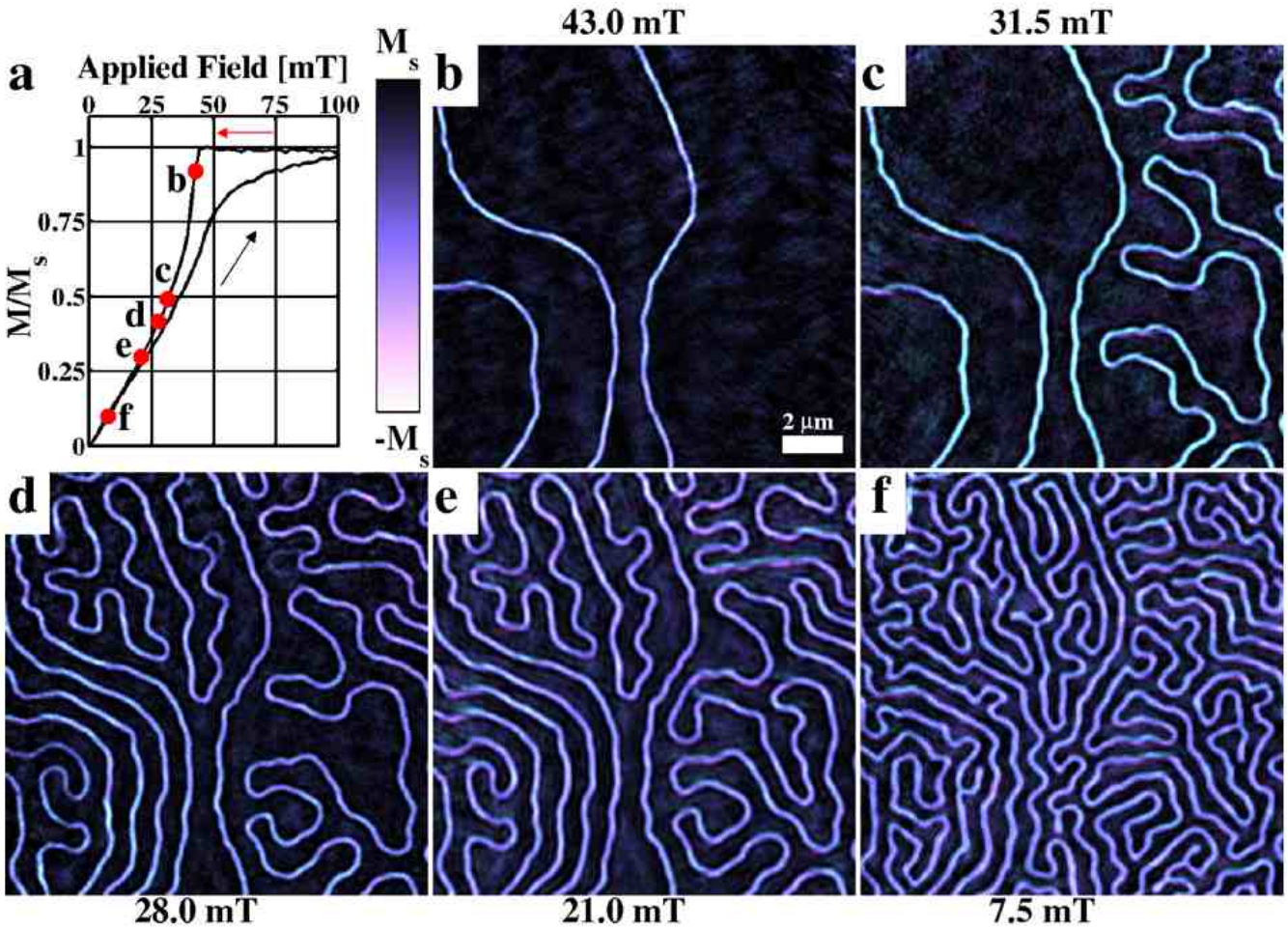

Domain evolution as the magnetic field was *decreased* from saturation towards zero. (a) Sample hysteresis loop as a function of applied field; (b-f) reconstructions from series of scanned diffraction patterns taken at various points in (a).

A. Tripathi, PNAS 108, 13393 (2011)

Coherent diffraction from crystals

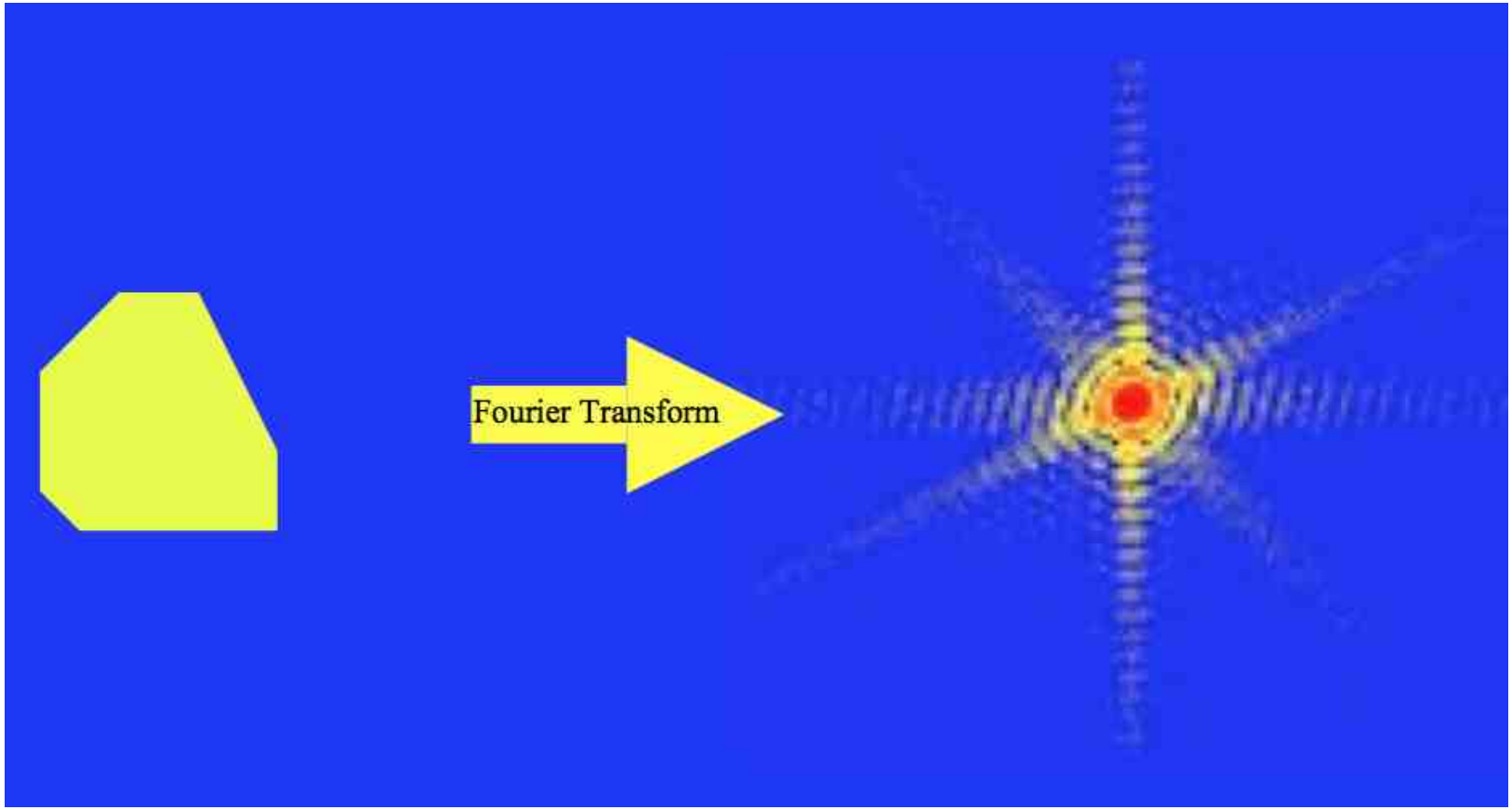

Coherent diffraction from crystals

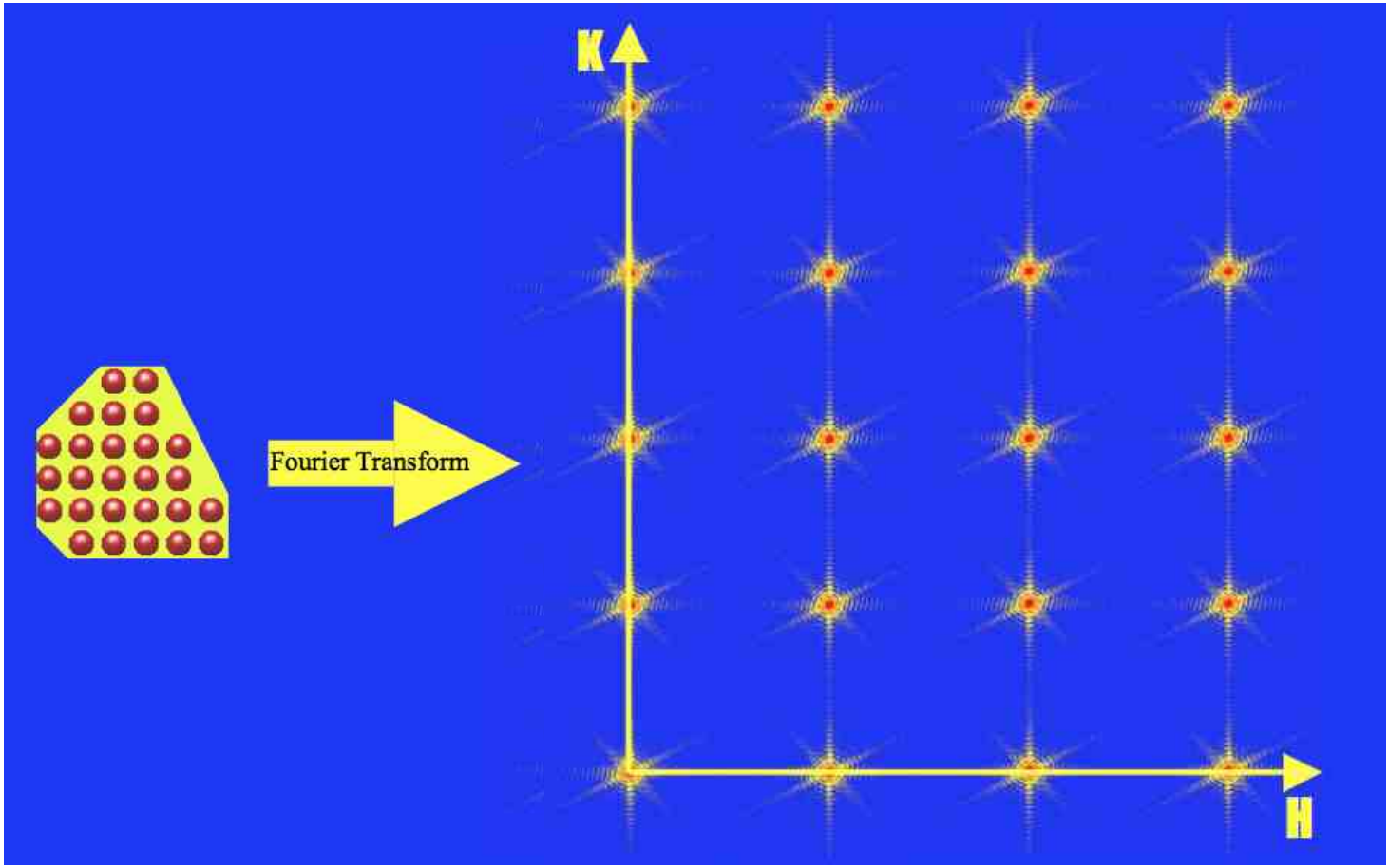

Asymmetries in the Bragg spots arise from lattice strain

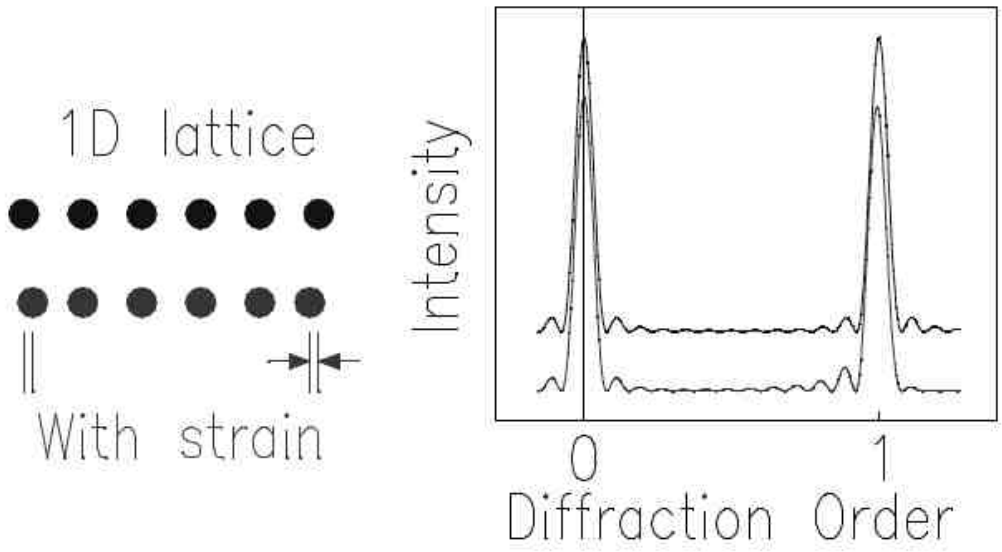

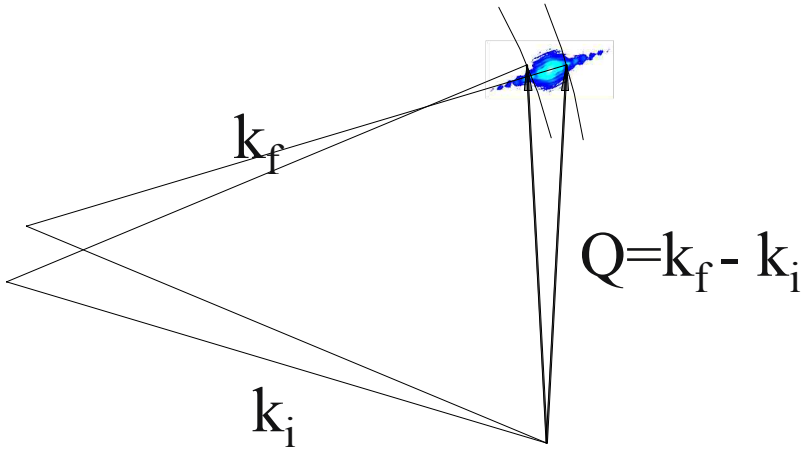

I. Robinson and R. Harder, *Nature* Mater. 8, 291 (2009)

Coherent x-ray diffraction in the Bragg geometry

- Coherent diffractive imaging (CDI) gives full complex amplitude from sample at a spatial resolution limited only by the detected scattered signal

- *Bragg CDI* is uniquely sensitive to crystalline order and lattice strain.

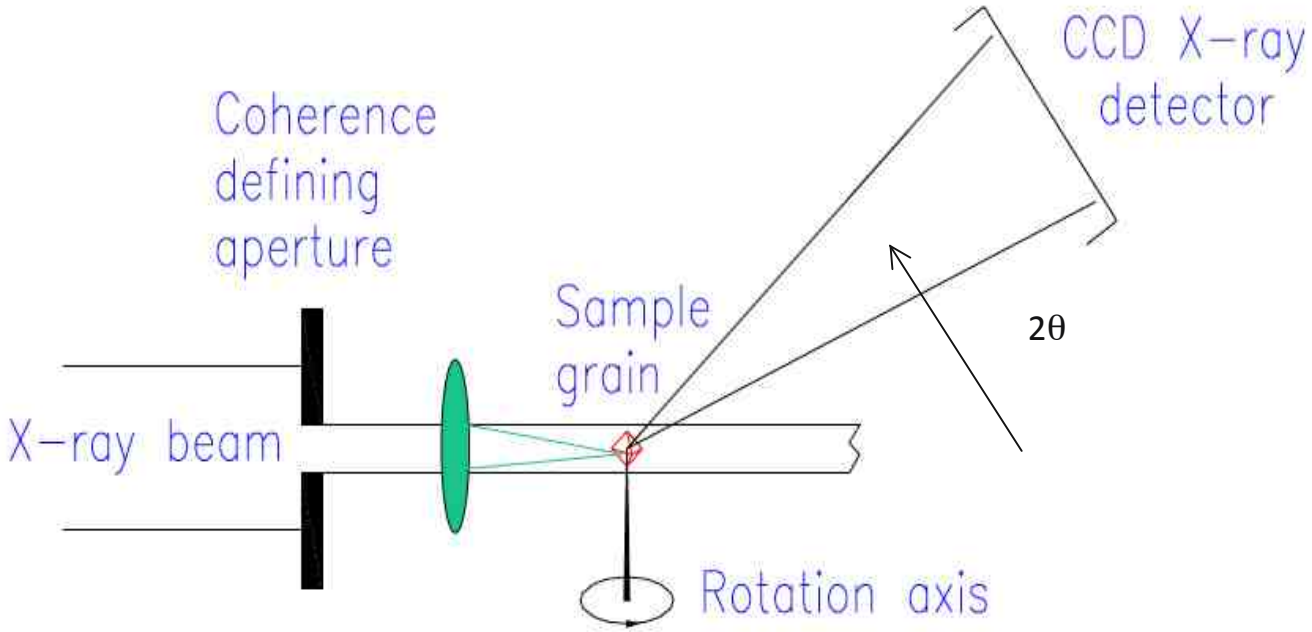

Three-dimensional Bragg method

- Select coherent part of hard x-ray beam with double crystal monochromator and precision slits
- Locate sample in beam and Bragg peaks (ideally, 3 to get complete strain tensor)
- Rock sample around Bragg peaks to record diffraction vs. angle
- Assemble 3D XYq data set, align to central peak
- Reconstruct via iterative phase retrieval, using constraint applied in pixel coordinates

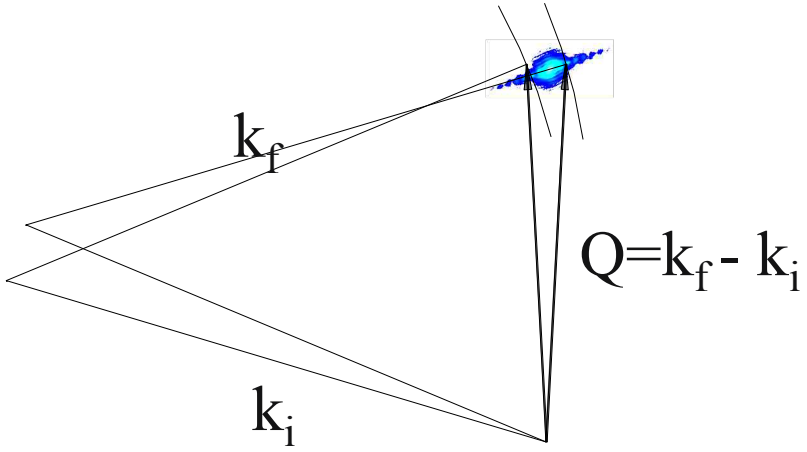

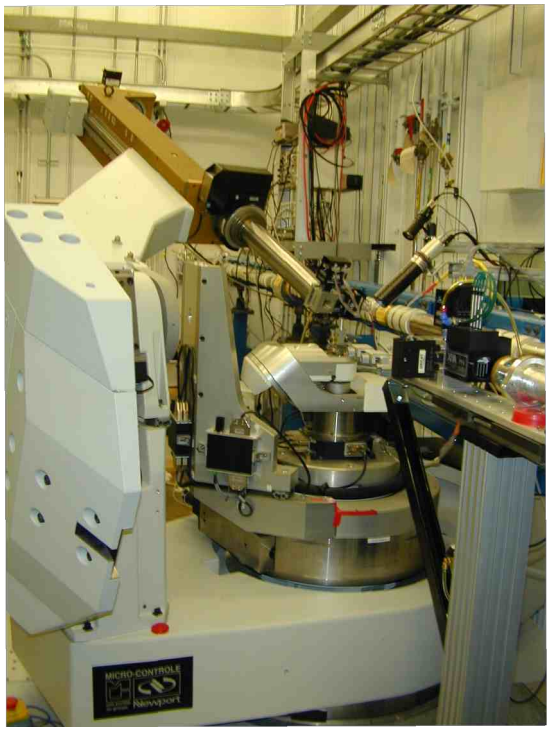

Setup at APS 34-ID-C beamline

Mapping crystal strain in 3D by CDI

0.5 μm Pb crystal grown on SiO_2 substrate

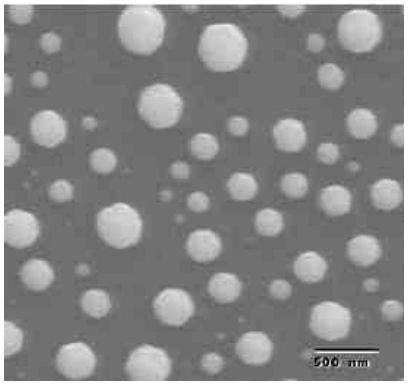

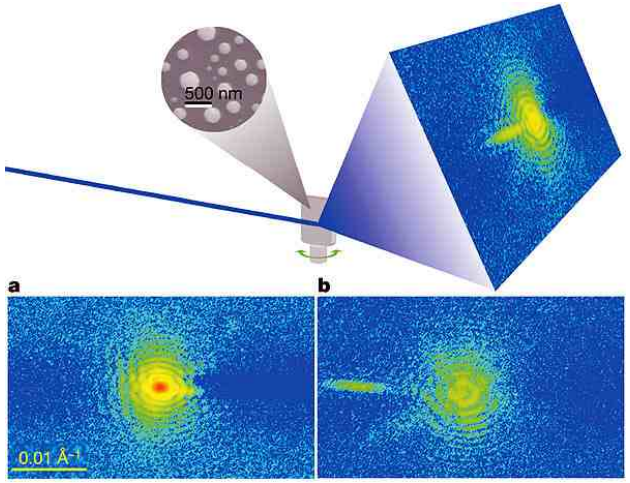

Map series of diffraction patterns about (111) Bragg peak

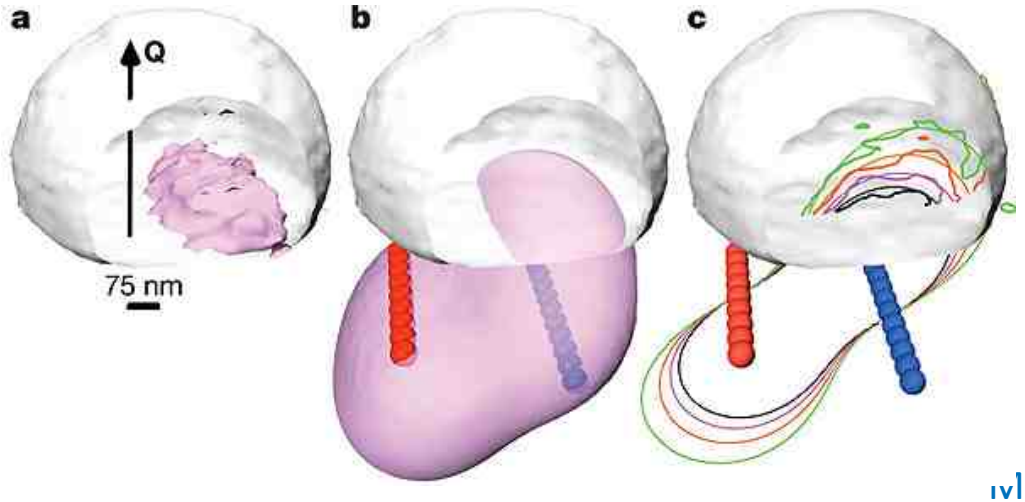

Reconstructed diffraction data

[iv] I. Pfeifer, Nature 442, 63 (2006)

3D strain is expressed as a tensor

$$\varepsilon_{ij} = \begin{bmatrix} \varepsilon_{xx} & \gamma_{xy} & \gamma_{xz} \\ \gamma_{xx} & \varepsilon_{yy} & \gamma_{yz} \\ \gamma_{xx} & \gamma_{yz} & \varepsilon_{zz} \end{bmatrix}$$

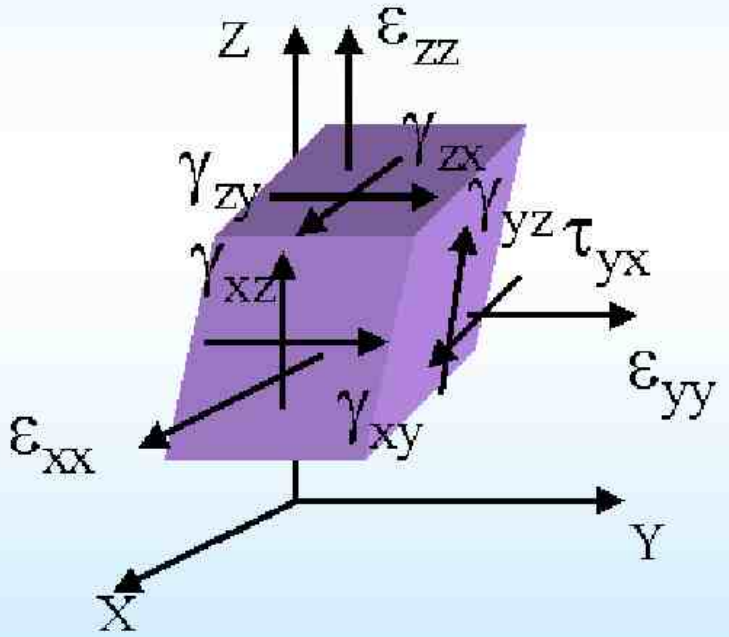

$$\varepsilon_x = \frac{\partial u_x}{\partial x} \qquad \varepsilon_y = \frac{\partial u_y}{\partial y} \quad , \qquad \varepsilon_z = \frac{\partial u_z}{\partial z}$$

$$\gamma_{yz} = \gamma_{zy} = \frac{\partial u_y}{\partial z} + \frac{\partial u_z}{\partial y} \quad , \qquad \gamma_{zx} = \gamma_{xz} = \frac{\partial u_z}{\partial x} + \frac{\partial u_x}{\partial z}$$

Vector displacement field around a lattice defect (Au crystal)

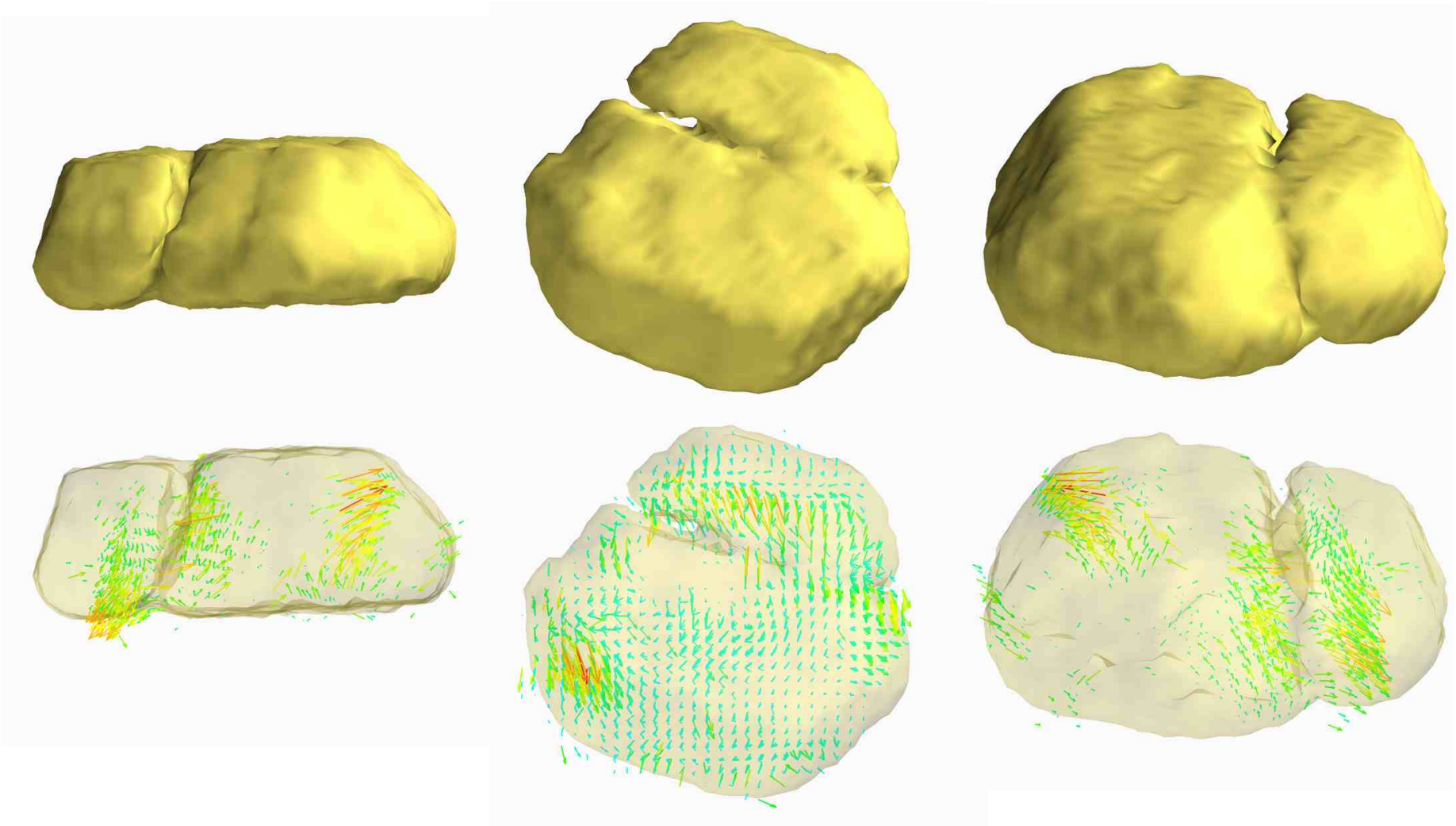

Produced by combining reconstructions from (11-1), (020), and (-111) reflections

3D strain map in ZnO nanorods

Nanoscale structures can be highly strained because of confinement effects, resulting in dramatically different electronic, magnetic and optical properties

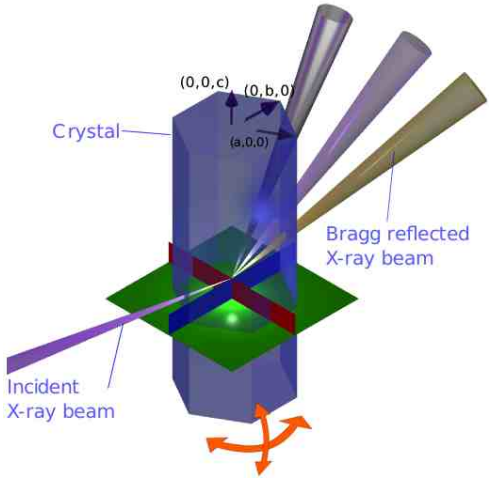

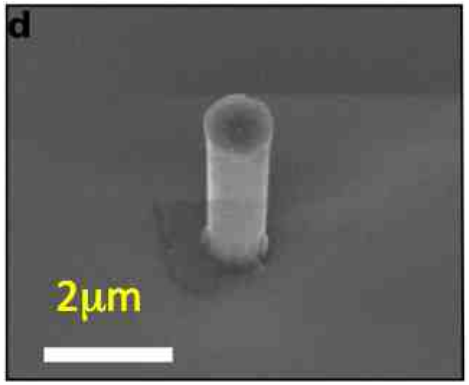

$$\epsilon_{ij} = \frac{1}{2}\left(\frac{\partial u_j}{\partial x_i} + \frac{\partial u_i}{\partial x_j}\right), \qquad \tau_{ij} = \left(\frac{\partial u_j}{\partial x_i} - \frac{\partial u_i}{\partial x_j}\right)$$

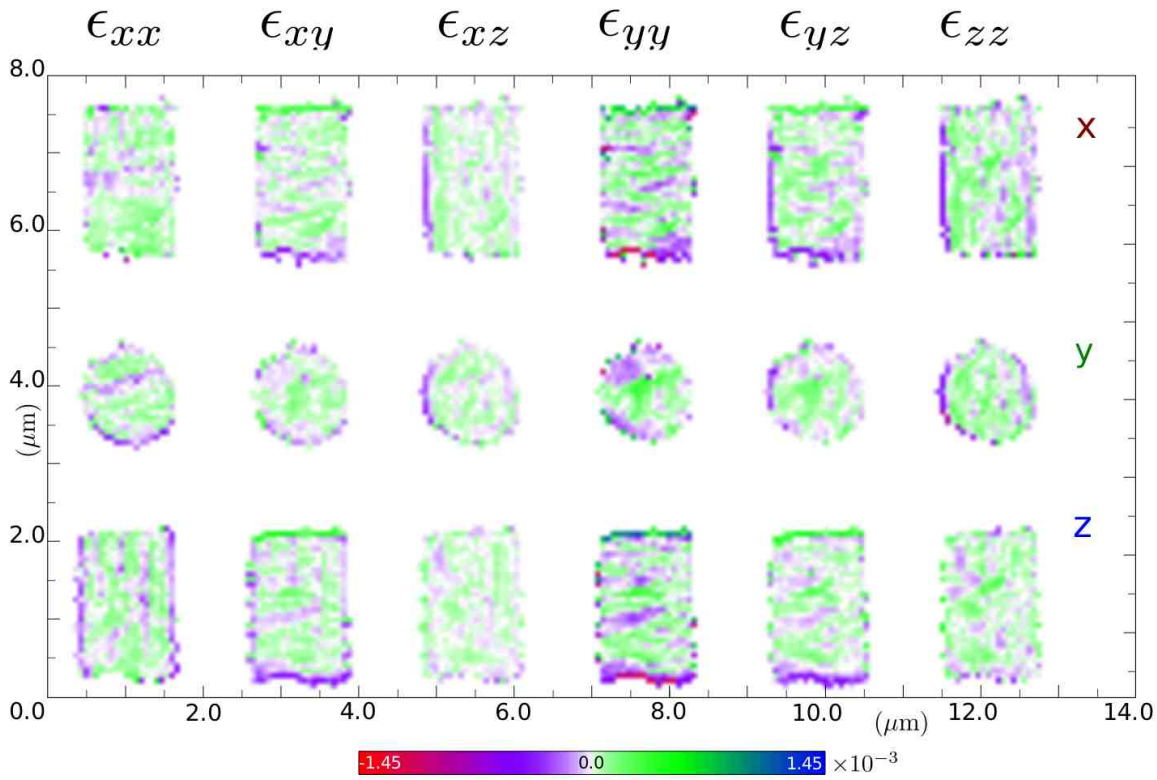

M. Newton, Nature Mater. 9, 120 (2010)

Holography

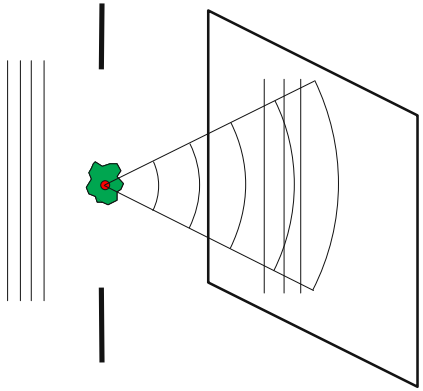

Gabor

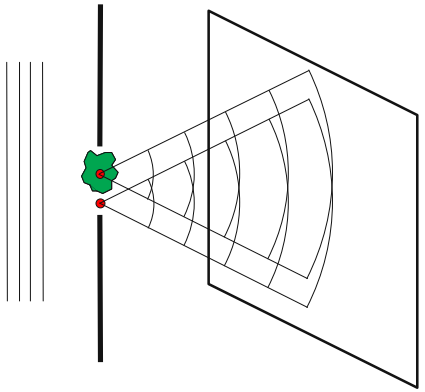

Fourier transform

Record hologram

$$I = |a+b|^2 = |a|^2 + |b|^2 + a^*b + ab^*$$

Reconstruct

$$\begin{aligned} bI &= b|a|^2 + b|b|^2 + a^*bb + abb^* \\ &= aI_b + b(I_a + I_b) + \text{background} \end{aligned}$$

- Reference wave encodes magnitude and phase of object wave
- Reconstruct object wave by "re-illuminating" hologram with reference wave (or its C.C.)

Gabor holography

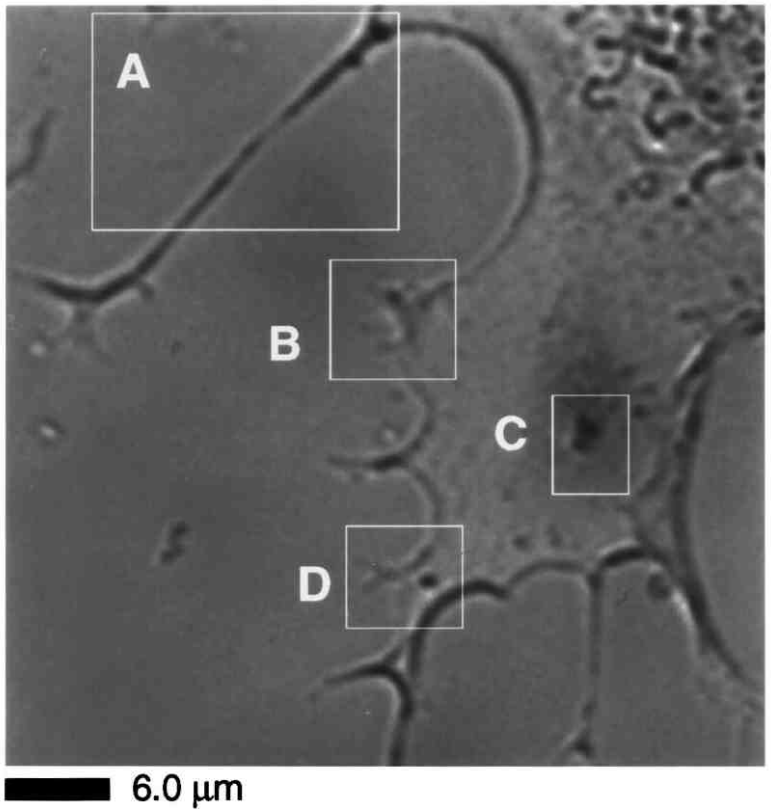

Visible light

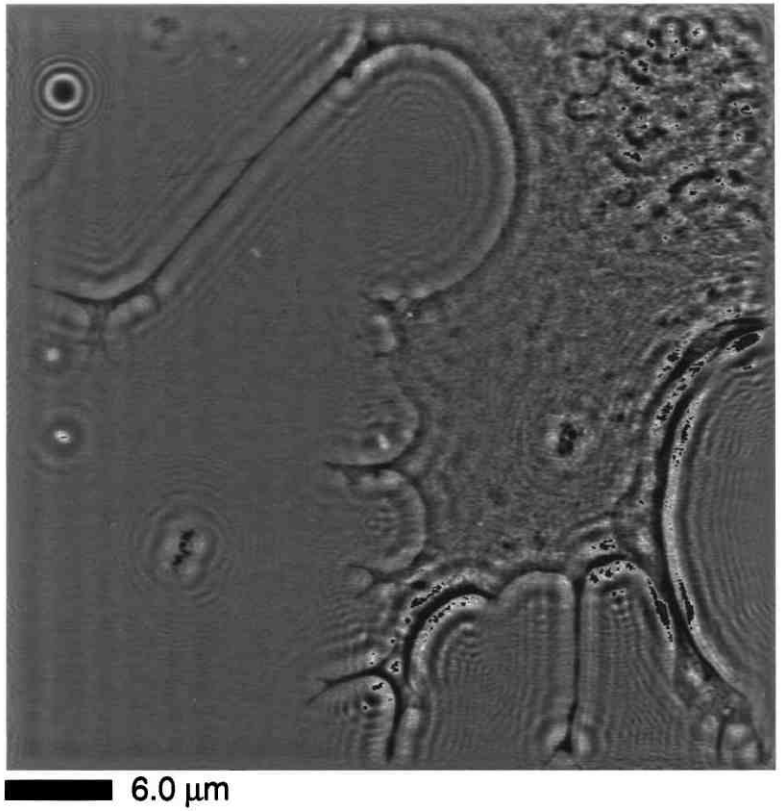

X-ray

Reconstructed hologram (right) of a NIL8 hamster neural fibroblast recorded with 656 eV x-rays. Estimated dose was 7.5 x105 Gy

S. Lindaas, JOSA A13, 1788 (1996)

FT hologram formation

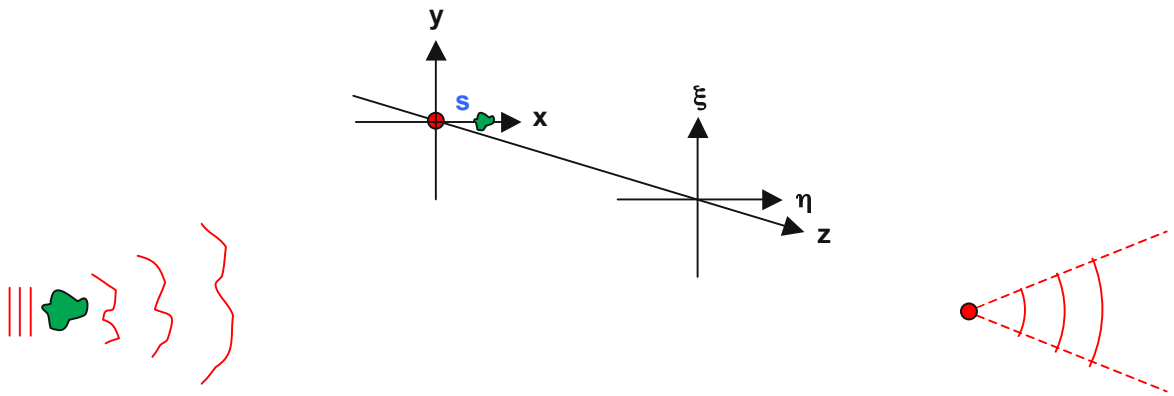

$$a(\xi,\eta) = \frac{e^{ikz}}{i\lambda z}\iint a(x-s,y)\; e^{\frac{ik}{2z}\left((x-\xi)^2+(y-\eta)^2\right)}\,dxdy$$

object wave

$$b(\xi,\eta) = \frac{e^{ikz}}{i\lambda z} b_0\, e^{\frac{ik}{2z}\left(\xi^2+\eta^2\right)}$$

reference wave

$$I = |a+b|^2 = |a|^2 + |b|^2 + a^*b + ab^*$$

hologram intensity

Reconstruction

- **Numerically take FT of hologram intensity to reconstruct**
- **Spatially separated primary, conjugate object waves result**
- **Weak curvature f(x,y) on object wave can be ignored**

Image terms: $$a^{*}b+ab^{*} = \varphi(s\xi)F(\xi,\eta)+\varphi(s\xi)^{*}F(\xi,\eta)^{*}$$

where: $$F(\xi,\eta) = \frac{e^{ikz}}{i\lambda z} f(\xi,\eta)\iint a(x,y)f(x,y)e^{-\frac{ik}{z}(x\xi+y\eta)}\,dxdy \quad ,$$

$$\varphi(s,\xi) = e^{-\frac{ik}{z}s\xi} \qquad \textbf{and} \qquad f(\xi,\eta) = e^{\frac{ik}{2z}(\xi^2+\eta^2)}$$

$$FT^{-1}\left\{a^{*}b+ab^{*}\right\} = f(x-s,y)\,a(x-s,y) + f(-(x-s),-y)^{*}\,a(-(x-s),-y)^{*}$$

UE56-SGM beamline and ALICE

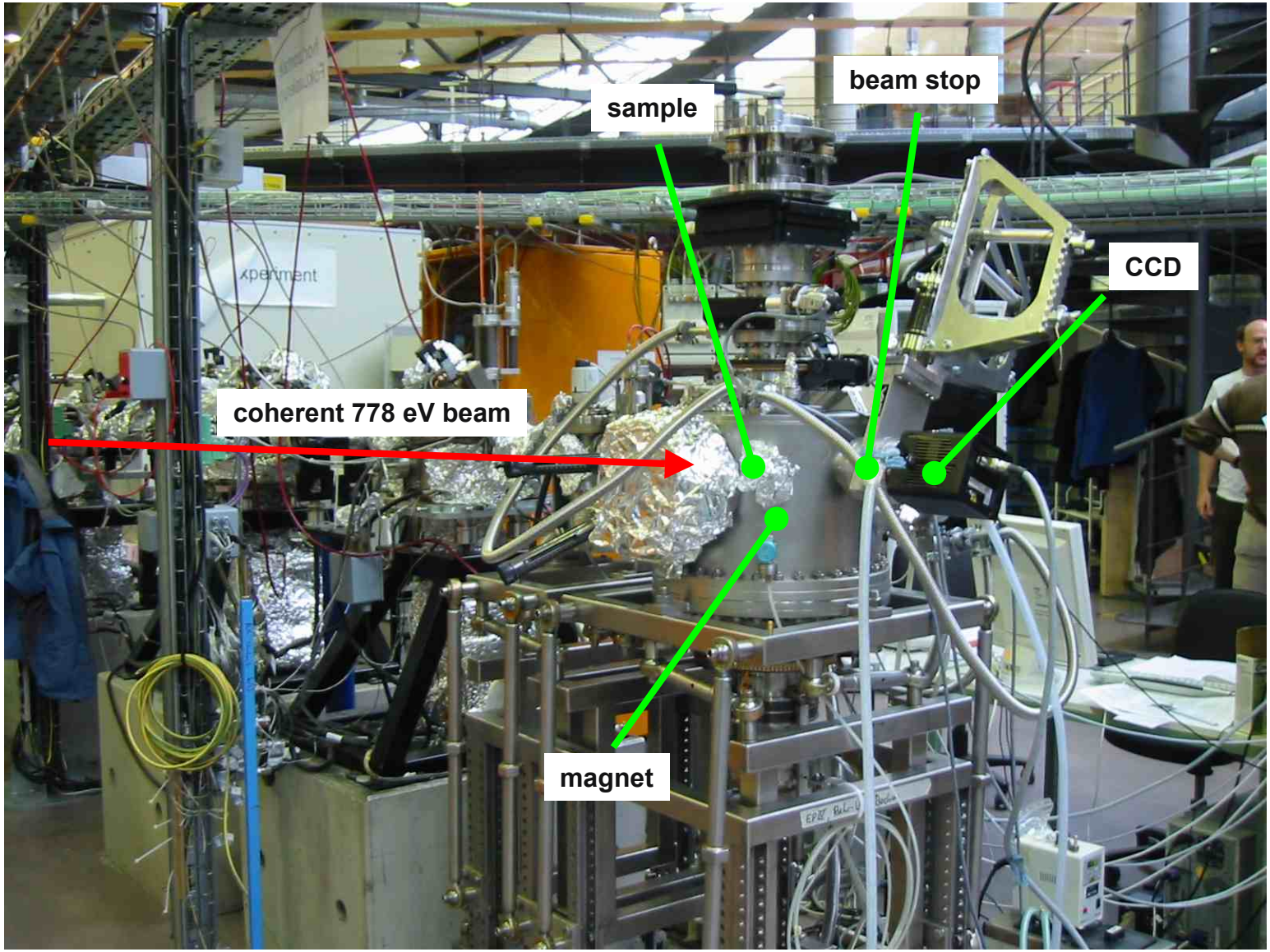

Fourier transform holography with a pinhole mask

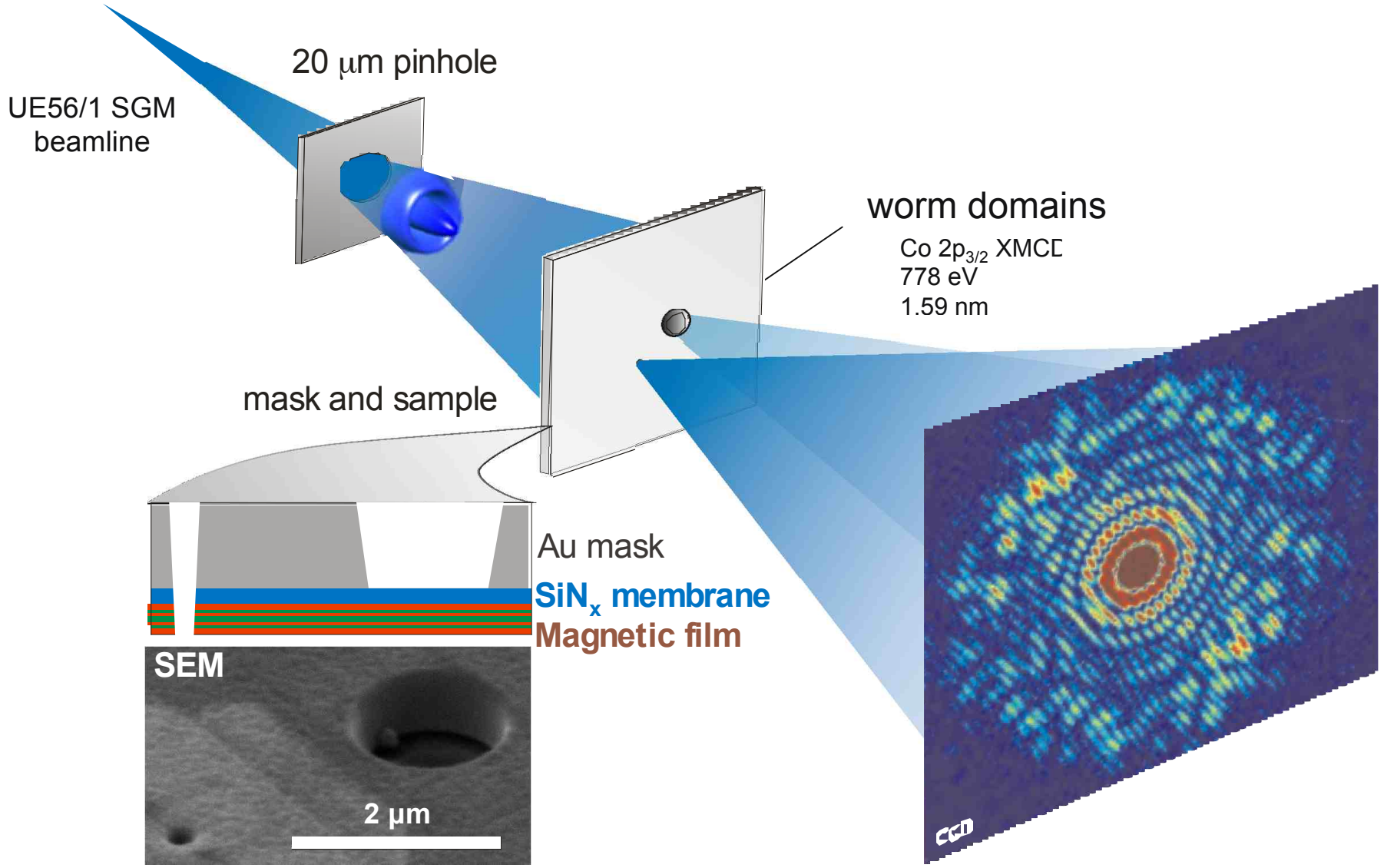

FTH

STXM

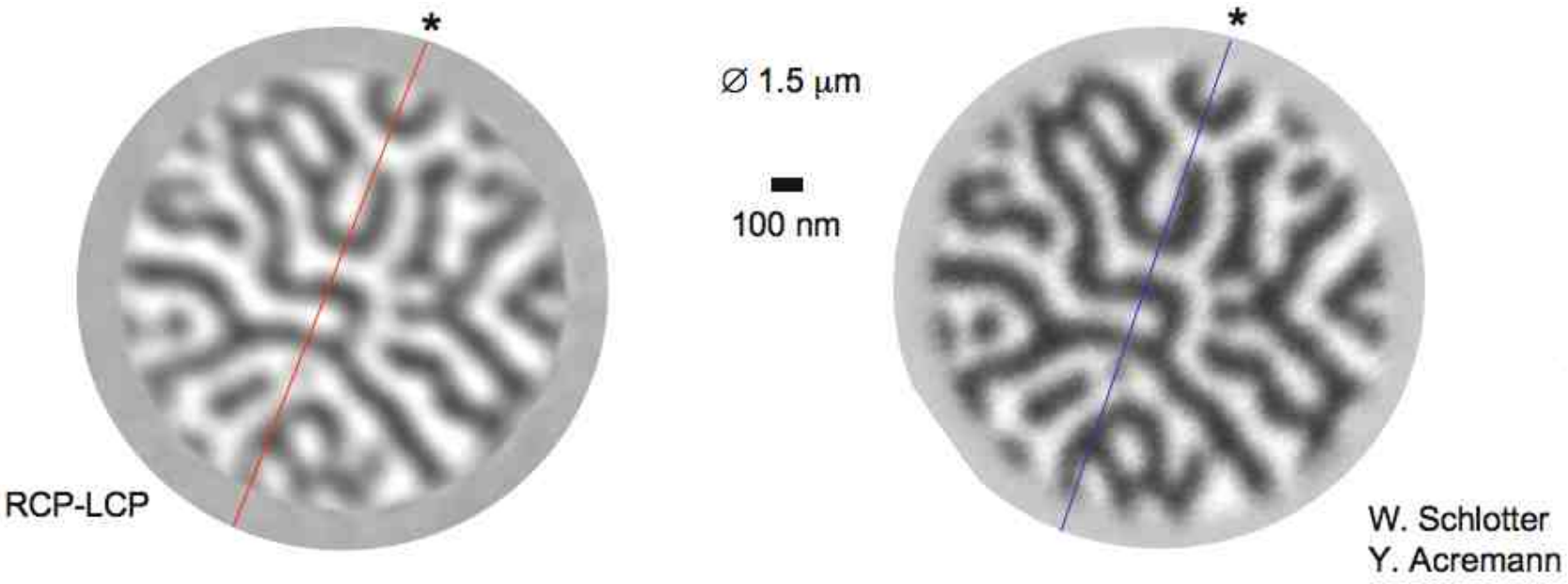

Reconstructed resolution ~50 nm

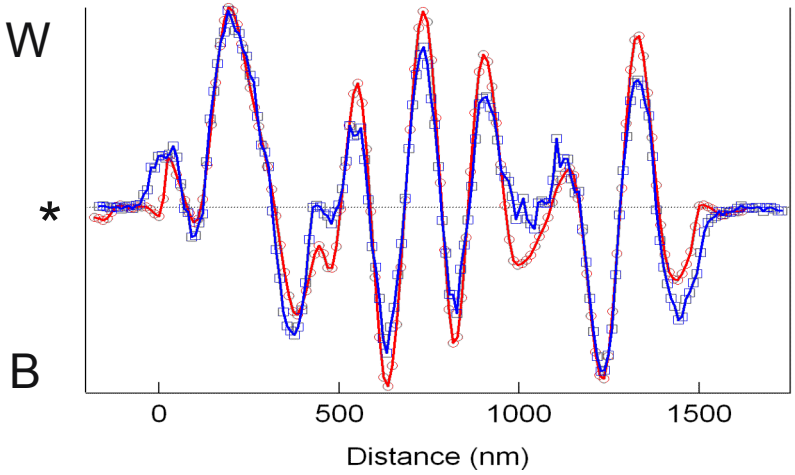

Resolution ~35 nm

S. Eisebitt,
Nature 432, 885 (2004)

Imaging resolution by x-ray holography

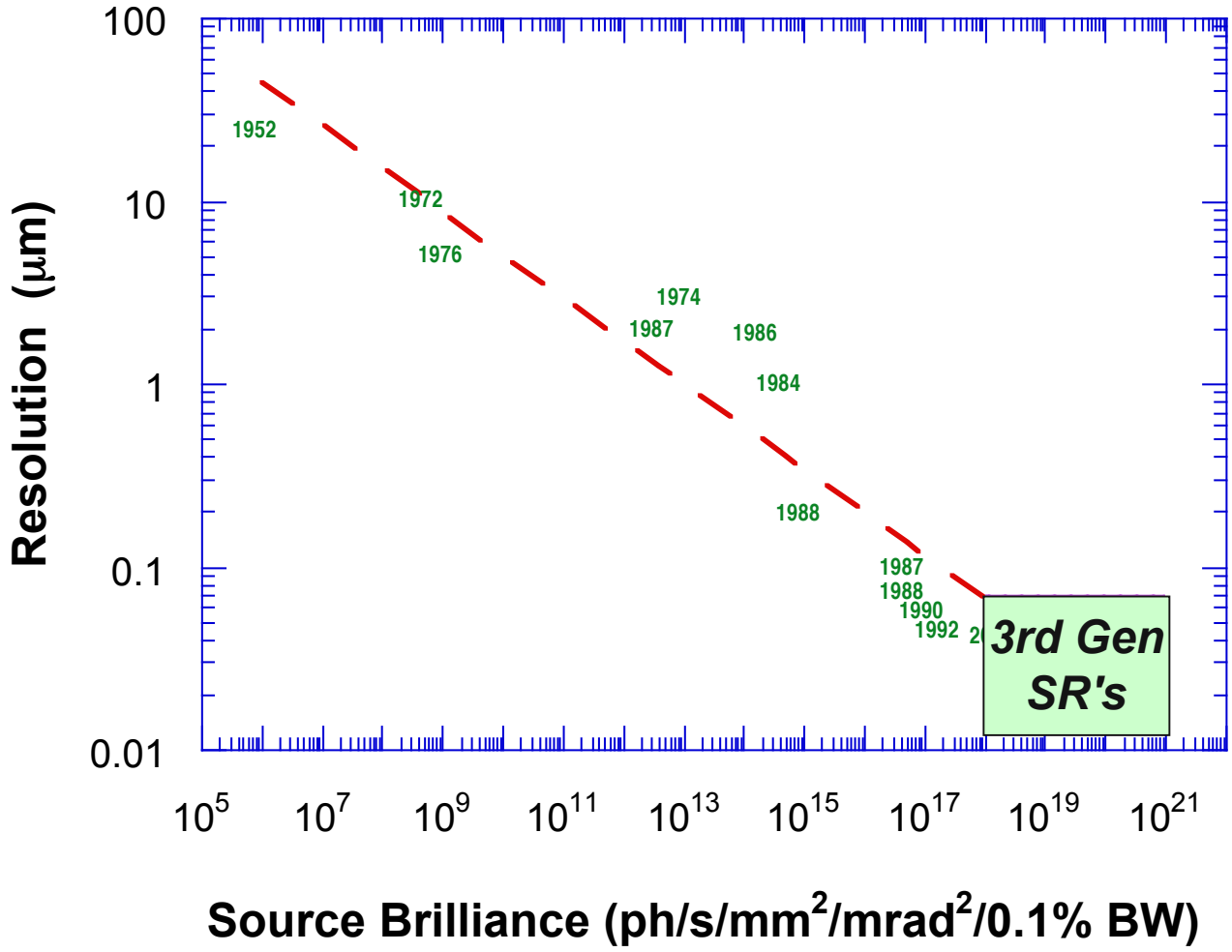

Pixel array detectors: a revolution in coherent imaging

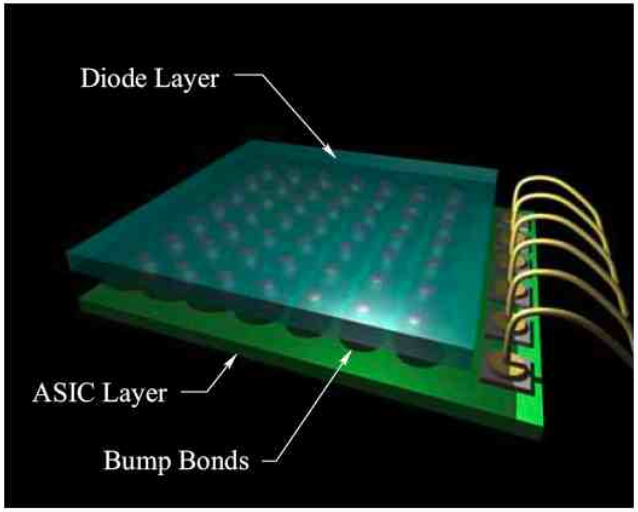

D. Schuette, S. Gruner (Cornell)

A Three Layer Hybrid Device

- Diode layer → converts x-rays to photocurrent.
- ASIC layer → custom signal processing electronics.
- A layer of metallic interconnects (bump bonds) between corresponding pixels on the diode and ASIC layers.

Pilatus 6M detector
(PSI/Dectris)

PADs can be read out in ~1 ms (CCDs take seconds!)

PAD pixels are currently ~150 µm. ~75 µm will be available next year

First ultrafast CDI of a virus with an x-ray laser

Linac Coherent Light Source at Stanford University, CA

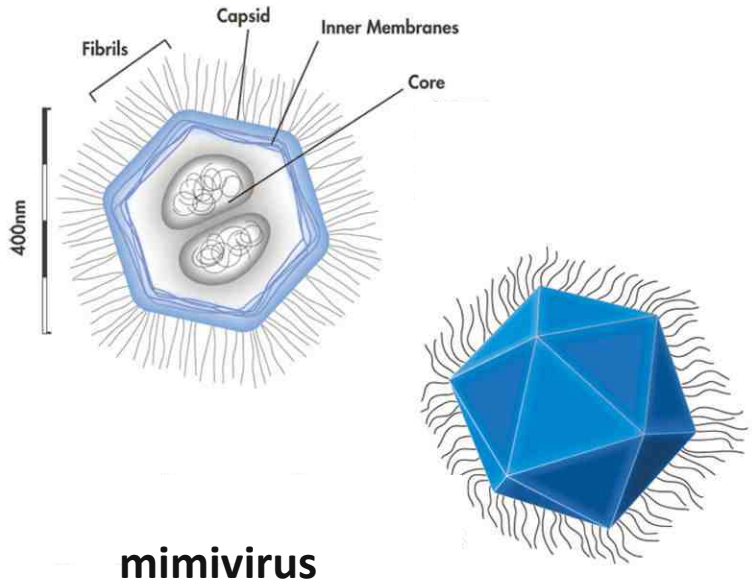

mimivirus

1.8 keV x-rays,
70 fs exposure !

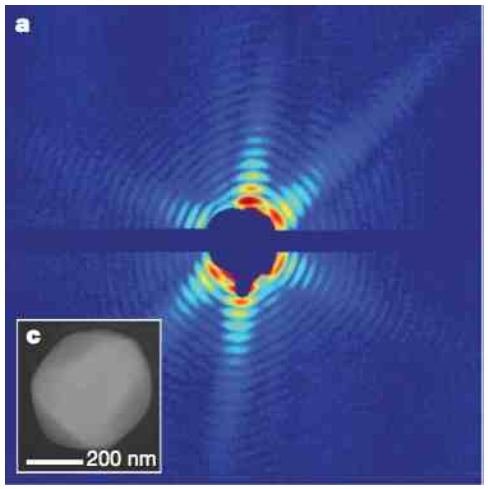

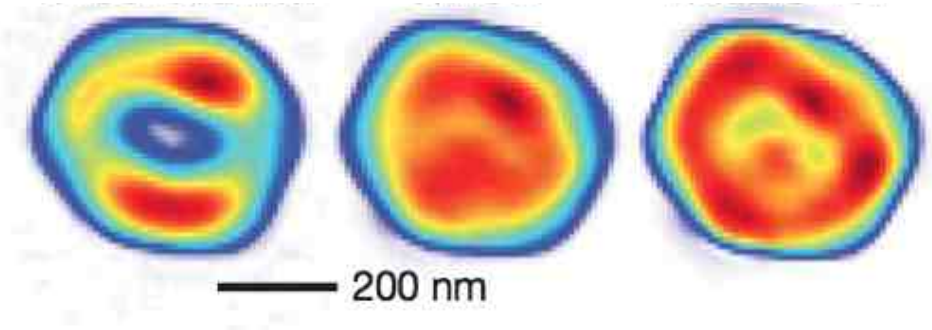

M. Seibert, Nature 470, 78 (2011)

CDI can be done on a tabletop!

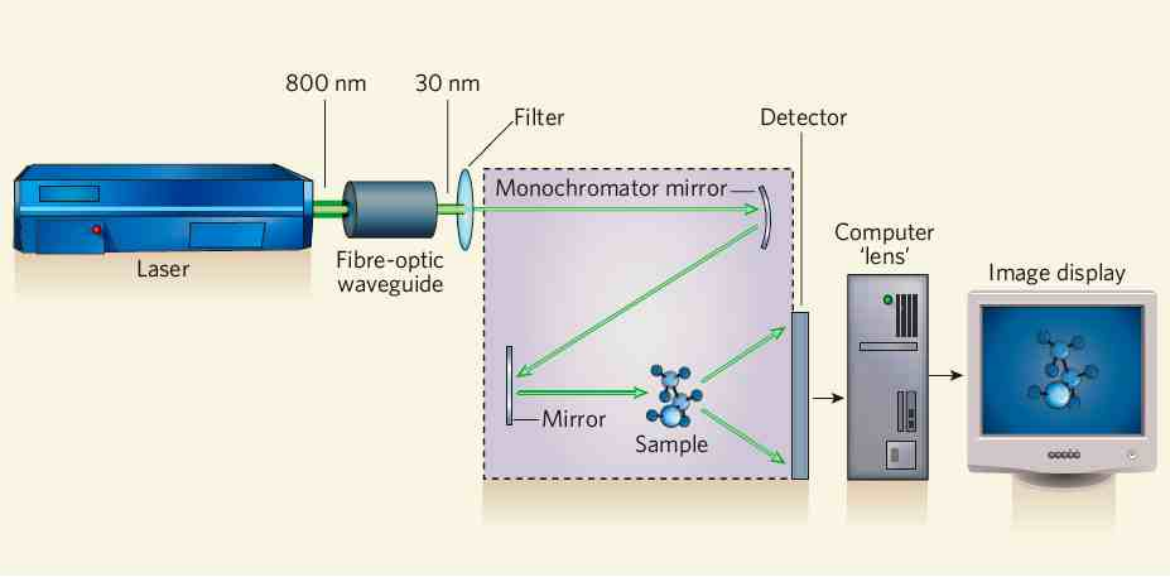

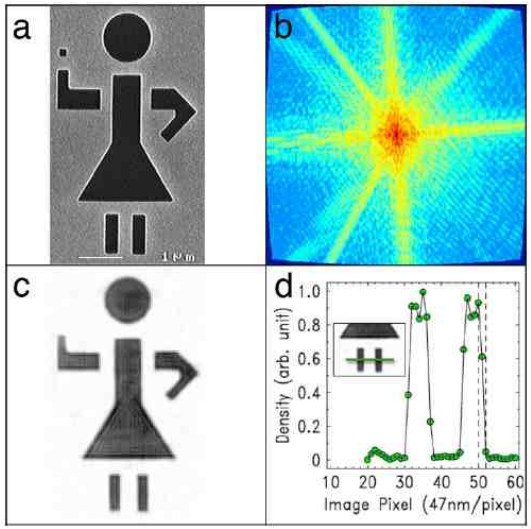

R. Sandberg, PRL 99, 098103 (2007)

R. Sandberg, PNAS 105, 24 (2008)

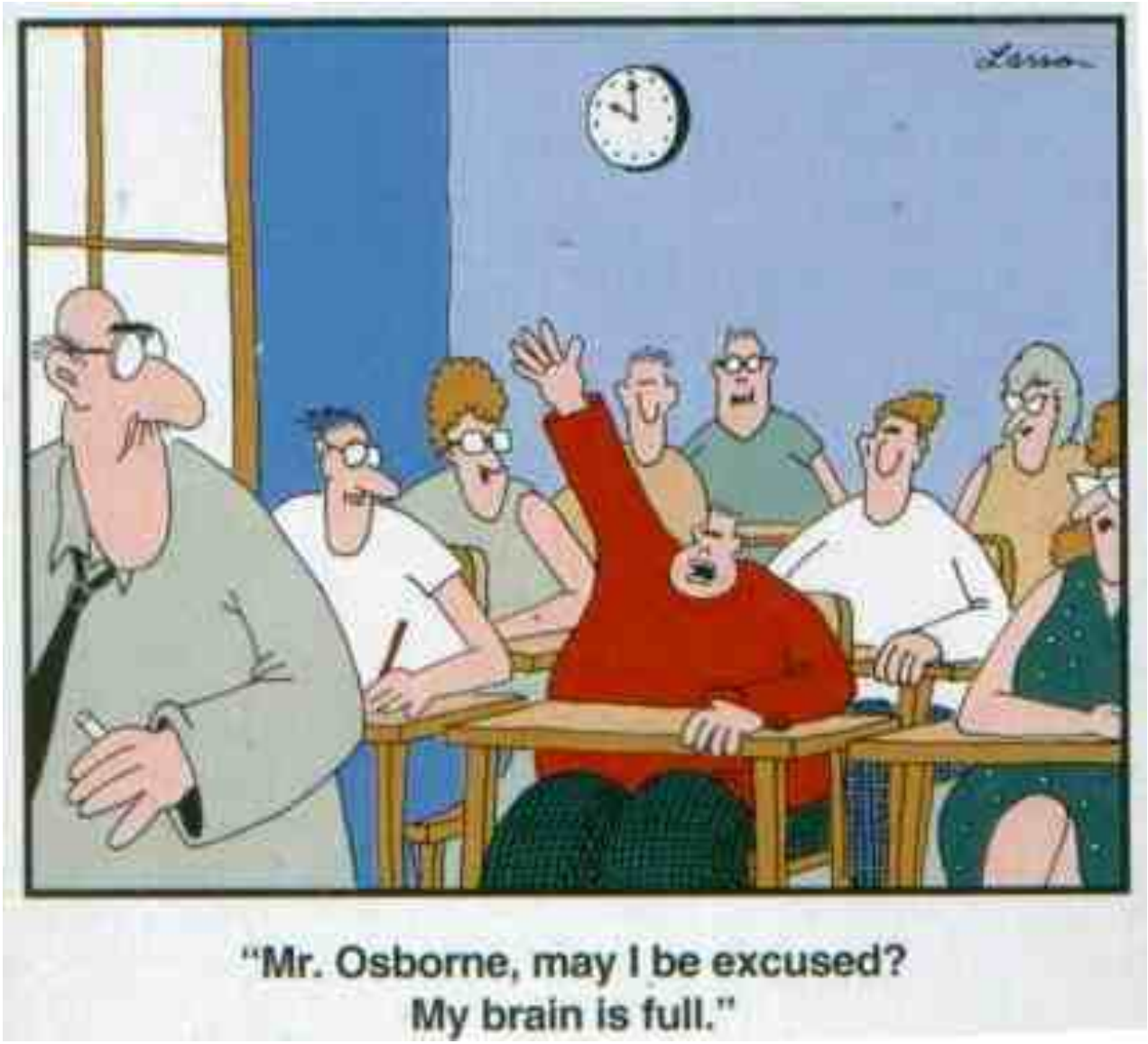
"Mr. Osborne, may I be excused?
My brain is full."

Summary

- **Resolution, contrast, sources, and optics for x-ray imaging**
- **Direct methods: projection, full-field, and scanning**
- **Indirect methods: microdiffraction, coherent diffraction, holography**

Many thanks to

Jonathan Lang

and to the many people who graciously shared their slides for these lectures

. . . and thank you!

Problems

1 Suppose you have a crystal with a c-axis lattice constant equal to 1 Å. What is the angle for the (001) Bragg reflection using 10 keV x-rays, and by how much is it shifted if the crystal is strained by that is strained by 0.5% ? What is the angle and shift for the (003) Bragg reflection?

2 Why would you use a Kirkpatrick-Baez mirror pair instead of a zone plate lens to focus a "white" (polychhromatic) x-ray beam for a Laue diffraction experiment? Why not?

3 A coherent x-ray beam of 8 keV energy and 2 µm diameter is incident on a disordered sample composed of 100 nm latex plastic spheres. The resulting x-ray speckle pattern is measured by a CCD x-ray camera at a distance of 3 m from the sample. What is the characteristic speckle size, and what is the radius of the first ring in the speckle pattern?

4 Suppose the sample in problem #3 is now a single, perfect crystal 100 nm in diameter. What is the characteristic size of the resulting Bragg reflections?

5 Do you expect sharp Bragg spots to be present in the coherent x-ray diffraction pattern from a biological cell that has been flash-frozen into a vitreous ice state? Why or why not?

6 Suppose you want to image ferromagnetic domains in a thin film of Fe using a transmission x-ray microscope. The x-ray beam is circularly polarized and the energy tuned to the L3 edge of Fe at 707 eV. How will the magnetic contrast measured using left-circular polarized x-rays differ from that using right-circular polarized x-rays? Now suppose you measure the coherent diffraction pattern from this sample. How will the diffraction patterns differ using left and right-circular polarized x-rays?